npj | precision oncology

Article

Published in partnership with The Hormel Institute, University of Minnesota

https://doi.org/10.1038/s41698-025-00815-x

Naltriben promotes tumor growth by activating the TRPM7-mediated development of the anti-inflammatory M2 phenotype

Viviane Nascimento Da Conceicao[1], Yuyang Sun[1], Manigandan Venkatesan[2], Jorge De La Chapa[1], Karthik Ramachandran[2], Rahul S. Jasrotia[3], Victor Drel[1], Xiufang Chai[1], Bibhuti B. Mishra[3], Muniswamy Madesh[2] ✉ & Brij B. Singh[1] ✉

Macrophage plasticity is critical for maintaining immune function and developing solid tumors; however, the macrophage polarization mechanism remains incompletely understood. Our findings reveal that Mg^{2+} entry through distinct plasma membrane channels is critical to macrophage plasticity. Naïve macrophages displayed a previously unidentified Mg^{2+} dependent current, and TRPM7-like activity, which modulates its survival. Significantly, in M1 macrophages, Mg^{2+} entry is facilitated by a novel Mg^{2}-dependent current that relies on extracellular Mg^{2+}, which was crucial for activating iNOS/NFκB pathways and cellular bioenergetics, which drives pro-inflammatory cytokines. Conversely, in M2 macrophages, Mg^{2+} entry occurs primarily through TRPM7 channels, pivotal for IL-4 and IL-10-mediated anti-inflammatory cytokine secretion. Notably, the Mg^{2+} deficient diet or addition of TRPM7 agonist Naltriben suppresses the M1 phenotype while promoting angiogenic factors and fostering tumor growth. These findings suggest that Mg^{2+} flux via specific channels is indispensable for macrophage polarization, with its dysregulation playing a pivotal role in tumor progression.

Modulating the immune response through changing macrophage polarization is a promising strategy to elicit beneficial outcomes such as removing pathogens and effective tissue repair[1,2]. The innate immune response depends on macrophage polarization that eliminate the invading pathogens directly via phagocytosis or via the production of cytokines[3–5]. Cytokines such as interferon (IFNγ), produced by lymphocytes, has been shown to transform naïve macrophages into activated macrophages (M1) that amplify the antigen-presenting capacity, complement-mediated phagocytosis, and secretes pro-inflammatory cytokines[6]. Release of pro-inflammatory mediators such as tumor necrosis factor (TNF)-α, IL-1, IL-6, and reactive nitrogen species from the M1 phenotype leads to a strong bactericidal and tumoricidal activity[7–10].

Similarly, T_H2-produced interleukin (IL)-4 could transform naïve macrophages into alternatively activated macrophages (M2). The M2 phenotype expresses molecules including Arginase1 (Arg1), which is involved in parasite infestation, tissue remodeling, and tumor progression[11,12]. Besides cytokines, alternative pathways have also been shown to modulate macrophage polarization; importantly, M2 polarization relies on oxidative phosphorylation and fatty acid oxidation; however, the mechanisms of how they modulate macrophage polarization are yet to be fully identified. In addition, the conventional M1/M2 classification of macrophages has been challenged[13], and perhaps a quick transition between M1 and M2 phenotypes is more appropriate. Thus, understanding factors common in macrophage polarization might dictate these key events. An Mg^{2+}-deficient diet also induced tumor growth, leading to metastatic spread[14]. Mg^{2+} plays a vital role in immune regulation and mitochondrial bioenergetics[15], and low serum Mg^{2+} is associated with a variety of chronic diseases, such as insulin resistance and type 2 diabetes, cancer development, metabolic syndrome, hypertension, cardiovascular disease, stroke, migraine, Alzheimer's disease, and asthma[16,17]. However, our understanding of its cellular regulation and clinical relevance in macrophage cells is not fully defined, as molecular components of Mg^{2+} homeostasis in different macrophage phenotypes remain undefined.

[1]Department of Periodontics, University of Texas Health San Antonio, San Antonio, TX, 78229, USA. [2]Center for Mitochondrial Medicine, Department of Medicine/Cardiology Division, University of Texas Health San Antonio, San Antonio, TX, 78229, USA. [3]Department of Developmental Dentistry, University of Texas Health San Antonio, San Antonio, TX, 78229, USA.
✉e-mail: muniswamy@uthscsa.edu; singhbb@uthscsa.edu

THE HORMEL INSTITUTE
UNIVERSITY OF MINNESOTA

Magnesium (Mg^{2+}) is the second-most abundant cation in cellular systems that plays a key role in various cellular responses. In immune cells, Mg^{2+} is a co-factor for immunoglobulin synthesis, C3 convertase. Similarly, Mg^{2+} is essential for immune cell adherence, antibody-dependent cytolysis, IgM lymphocyte binding, macrophage response to lymphokines, and T–B cell adherence[18,19]. Intracellular Mg^{2+} can also function as a second messenger in the immune activation of T and B lymphocytes[16]. Similarly, Mg^{2+} levels also regulate cytokine production, which plays a leading role in macrophage function, and loss of Mg^{2+} has been shown to induce autoimmunity[20]. Several Mg^{2+} permeable ion channels and transporters have been identified, and their characterization could provide new insights into the regulation of Mg^{2+} homeostasis and how it affects immune responses[21]. Importantly, deletion of Mg^{2+} channel TRPM7 in chicken DT40 B lymphocytes becomes growth deficient, leading to cell death within 48 hours[22]. TRPM7 deficiency in mice results in early embryonic lethality, and murine TRPM7$^{-/-}$ thymocytes experience a developmental block, suggesting a critical role of TRPM7 in cell physiology[23,24].

Additionally, genetic mutations of the intracellular Mg^{2+} regulator, *MAGT1*, have been shown to elicit specific immune defects in affected individuals (XMEN—*X*-linked immunodeficiency), suggesting that Mg^{2+} regulation is essential for immune function[25]. Similarly, SLC41 and TMEM63 are also shown to increase Mg^{2+} entry, but their role in immune cells is not known[26]. Thus, identifying the precise function of these Mg^{2+} entry channels in various immune cells and establishing the mechanisms of immune regulatory networks are critical in modulating the immune response.

This study is aimed to identify and characterize the Mg^{2+} entry channels/transporters in various macrophage phenotypes. Our data suggests that Mg^{2+} homeostasis in naïve and M2 macrophages is primarily mediated through TRPM7, which is critical for tumor development. In contrast, the M1 phenotype depended on an unidentified plasma membrane Mg^{2+} entry channel. Mice fed a diet deficient in Mg^{2+} had reduced M1-type macrophages and promoted tumor growth. Finally, loss of TRPM7 specifically prevented M2 polarization without affecting the M1 phenotype, along with a decrease in critical anti-inflammatory cytokines. Moreover, activation of TRPM7 was sufficient to promote M2 polarization and promotes tumor progression. These results suggest that differential expression of Mg^{2+} entry channels and transporter is essential for M1/M2 function in modulating tumor development and progression.

Results

Mg^{2+} entry shapes cytotoxic M1 activity and inhibition of tumor development

Macrophages have a dual role in tumor development, where M2 cells promote tumor progression, whereas M1 cells produce cytokines that inhibit tumor progression[27]. Thus, to evaluate the role of Mg^{2+} entry in different macrophage phenotypes and its role in solid tumor growth, we randomized nude mice in our experimentation, as they lack the T and B cells. The first cohort was given the Mg^{2+} supplemented diet, whereas the other cohort was put on an Mg^{2+} deficient diet (Fig. 1A). Interestingly, the solid tumors grew significantly more in Mg^{2+} deficient diet, when compared with Mg^{2+} supplemented diet (Fig. 1B). Increased tumor volume was observed in mice placed on a Mg^{2+} deficient diet (Fig. 1B, C). Using flow cytometry, we evaluated the presence of the M1 and the M2 phenotype in both Mg^{2+} supplemented and Mg^{2+} deficient diets. Interestingly, fewer M1-positive cells were observed in animals placed on the Mg^{2+} deficient diet when compared with Mg^{2+} supplemented diet (Fig. 1D, E). In contrast, the number of M2 cells was not significantly affected (Fig. 1D). Confocal microscopy further confirmed the immunohistochemical data, where an increase in M1 cells was observed in Mg^{2+} supplemented diet, whereas the number of M2 cells were increased in Mg^{2+} deficient diet (Fig. 1E). Next, we evaluated the characteristics of the Mg^{2+} entry channel using in vivo conditions and macrophages isolated from solid tumors showed the initiation of a Mg^{2+} current, which was significantly higher in macrophages isolated from Mg^{2+} deficient diet that shows the M2 phenotype (Fig. 1D-F). Significantly, the Mg^{2+} currents reversed at 0 mV, which is consistent with the previous recording observed with TRPM7 channels[28,29] (Fig. 1F). Furthermore, the tumor growth factors VGEF were also decreased in Mg^{2+} supplemented diet (Fig. 1G), along with a decrease in pro-inflammatory cytokines, without affecting the M2-dependent cytokines (Fig. 1G). We next estimated serum Mg^{2+} levels, which were significantly decreased in mice subjected to Mg^{2+} deficient diet, even though the TRPM7 channel activity was higher (Fig. 1H). These results suggest a crucial role for Mg^{2+} transport in distinctly modulating the immune response.

Identification and characterization of Mg^{2+} entry channels in naïve macrophages

Next, we characterized the Mg^{2+} entry channels in primary macrophage cells. The bone marrow of wildtype (C57) mice was used to isolate primary macrophage cells and cultured them in conditioned media. Naïve macrophages (Mφ) were analyzed by flow cytometer, and only F4/80^{+} and CD11b^{+} positive cells were used for all experiments (Supplementary Fig. 1A). To address the role of Mg^{2+} in the survival/proliferation of naïve Mφ, we treated these cells with low (0–0.5 mM) and high (1–20 mM) Mg^{2+} concentrations (Fig. 2A, B). Importantly, a decrease in the cell proliferation of naïve Mφ was observed when cells were deprived of Mg^{2+} (Fig. 2B; Supplementary Fig. 1B). In contrast, increasing concentrations of external Mg^{2+} showed higher cell proliferation/viability (Fig. 2B). Further, to establish the role of Mg^{2+} in Mφ function, RNA-seq analysis was performed on Mφ cultured in high and low [Mg^{2+}], which showed a differential expression of genes under low (0.1 mM) and high (2.0 mM) Mg^{2+} (Fig. 2C, D; and Supplemental Table 1). Pathway analysis revealed that genes that were crucial for immune function as well as their ability to withstand stress were increased in high [Mg^{2+}]; whereas, IL4 pathway and type 2 immune response were increased in low [Mg^{2+}] (Fig. 2E). These results are consistent with previous findings[30,31] and suggest a crucial role for Mg^{2+} entry in modulating Mφ proliferation/survival and assisting in their polarization.

We next focused on characterizing the transporter/channels that could contribute to Mg^{2+} entry in naïve Mφ. Decreasing intracellular Mg^{2+} led to the activation of Mg^{2+} entry and an outward rectifying current elicited by a voltage ramp protocol ranging from −100 to +100 mV (Fig. 2F, G). The outwardly rectifying currents reversed close to 0 mV, consistent with the previous recording observed with TRPM6/7 channels[28,29]. To further separate if the Mg^{2+} currents observed are through TRPM6 or TRPM7 channels, we exploited the differential effect of 2-APB on these channels as 2-APB activates TRPM6, but inhibits TRPM7 currents[16,32]. Mg^{2+} current amplitude was substantially reduced by the addition of 2-APB (50 μM; Supplementary Fig. 1C); furthermore, a TRPM7-specific inhibitor (NS8593) also had a similar effect on the Mg^{2+} current amplitude (Fig. 2F–H). Furthermore, the addition of Ca^{2+} in the external media also showed similar current properties; however, the inward current amplitude was slightly higher in the presence of Ca^{2+} (Supplementary Fig. 1D, E). Pretreatment of naïve Mφ with a nonspecific Ca^{2+} channel blocker (SKF96365) also showed a decrease in TRPM7 currents (Supplementary Fig. 1F, G), suggesting that TRPM7 is one of the channels that initiate Mg^{2+} entry in naïve Mφ. As increased proliferation and survival were observed at higher external Mg^{2+} levels, we evaluated the TRPM7 current properties at higher Mg^{2+} levels. Surprisingly, increasing external Mg^{2+} showed a decrease in TRPM7 currents, and a dose-dependent reduction in TRPM7 currents was observed when external Mg^{2+} levels were gradually increased (Fig. 2I–K).

These results contrast the cell proliferation data and suggest that perhaps additional Mg^{2+} entry channels in naïve Mφ could modulate Mg^{2+} entry. Importantly, *TRPM7*$^{-/-}$ cells have been shown to have regular Mg^{2+} influx[33], suggesting that another channel/transporter could also be critical for Mg^{2+} entry. Thus, we next evaluated this unknown Mg^{2+} entry channel. In naïve Mφ increasing external Mg^{2+} led to a gradual increase in intracellular Mg^{2+} levels (Fig. 2L; Supplementary Fig. 1H), which was not blocked by the addition of gadolinium (Gd^{3+}), a known non-specific divalent cation

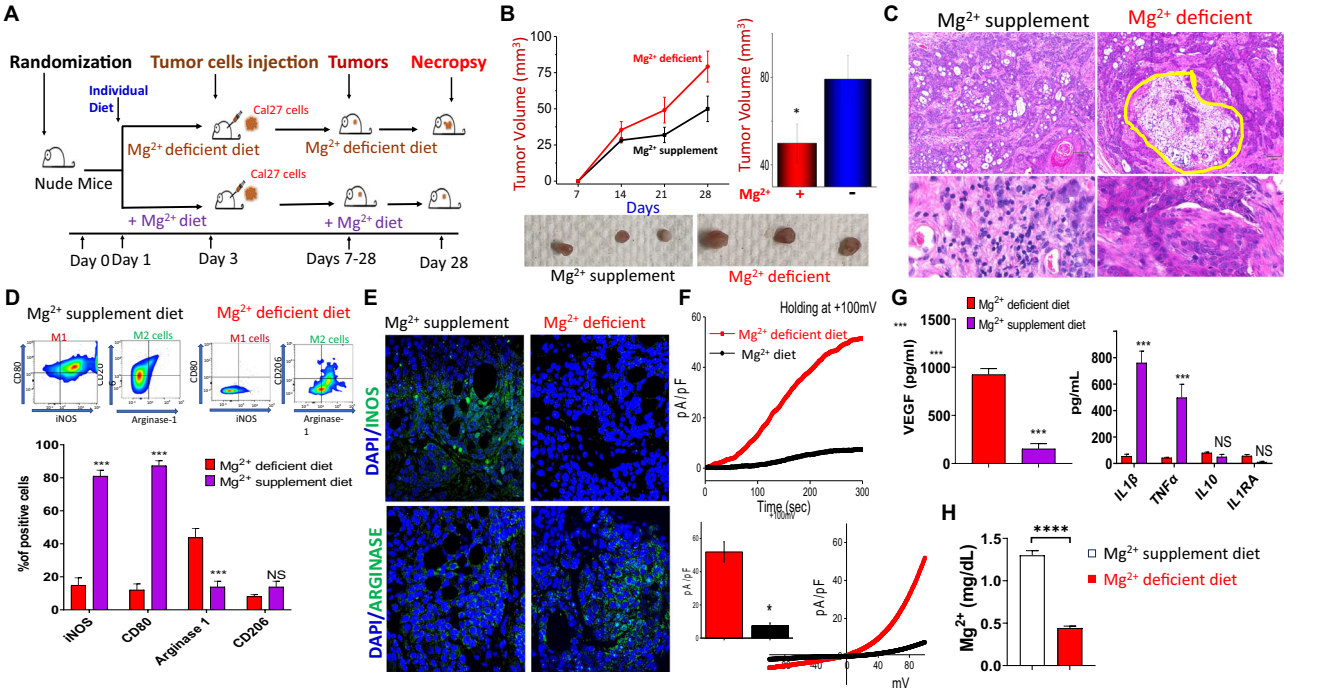

Fig. 1 | Mg^{2+} deficient diet decreases M1 macrophage cells and promote tumor growth. Schematic overview of mice diet study, on day 0, mice were put on an Mg^{2+} deficient diet and an Mg^{2+} normal diet. On day 3, 3×10^6 Cal27 cells were injected into the mice, and tumor growth was measured every week. On day 28, mice were sacrificed for tumor collection (**A**). Tumor volumes were measured using a digital caliper every 7 days using a Xenograft tumor model protocol. The data shown are representative of three independent experiments with similar results. Tumor volumes are depicted in the picture. Bar graphs depict average ± SD for relative values, NS = non-significant (Student's *t*-test) (**B**). The pictures shown below are isolated solid tumors from mice, and (**C**) shows microscopy analysis showing H&E staining of tumors from the Mg^{2+} deficient diet and Mg^{2+} normal diet. **D** Flow cytometer analysis on nude mice tumors from Mg^{2+} deficient diet, and Mg^{2+} normal diet was performed to measure the levels of surface markers to demonstrate the efficacy of cell infiltration. Data show low arginase and $CD206^+$ M2 markers and high $CD80^+$ and iNOS M1 markers to illustrate successful M1 infiltration on Mg^{2+} normal diet and low levels of both markers when mice were given Mg^{2+} deficient diet. Bar graphs show the percentage of M1 and M2 markers (average ± SD for relative values, $^{***}p \le 0.001$ (Student's *t*-test)) on different diets, from three independent experiments (**E**). Expression analysis showing the level of expression of arginase 1 and iNOS of mice placed on Mg^{2+} sufficient diet (normal) or Mg^{2+} deficient diet. **F** Representative whole-cell recording showing outward currents at +100 mV from macrophages isolated from tumor cells (n = 6) in mice placed on Mg^{2+} sufficient diet or Mg^{2+} deficient diet. IV curves (acquired when currents reach peak) under various conditions are also shown. A bar graph (average ± SE) showing the quantification of the current is also shown. **G** VGEF in tumors from the Mg^{2+} deficient diet and Mg^{2+} normal diet. The data shown are representative of three independent experiments. $^{***}p \le 0.001$. Bar graphs represent quantification (± SD) of tumor cytokines present from the Mg^{2+} deficient diet and the Mg^{2+} normal diet. The data shown are representative of three independent experiments. $^{***}p \le 0.001$, NS = non-significant (Student's *t*-test). **H** Quantification (bar graphs ± SE) of serum Mg^{2+} levels in Mg^{2+} deficient diet and Mg^{2+} supplemented diet. $^{****}p \le 0.005$ (Student's *t*-test).

inhibitor[34], or the addition of either 2-APB, SKF96365, or flufenamic acid (FFA, a TRPM channel inhibitor)[35] (Supplementary Fig. 1I-L). We also evaluated the current properties of this unique Mg^{2+} channel, which showed that a linear current is evoked by the presence of external Mg^{2+} and increasing external Mg^{2+} levels, leading to a gradual increase in Mg^{2+} currents (Fig. 2M–O). The IV relationship was not altered upon increasing Mg^{2+} concentrations, and in naïve Mφ, the currents reversed between -10 and 0 mV (Fig. 2N), which is slightly different from that observed with MagT1 or Tmem63b[36]. Supplementation of Ca^{2+} or Ba^{2+} did not show the activation of these currents, which is different from both MagT1 and Tmem63b currents, suggesting that it is a different Mg^{2+} entry channel (Supplementary Fig. 1M). To further establish the molecular identity of the channel, we silenced the known Mg^{2+} channels. Silencing of Slc41A/B/C or Tmem63b did not decrease Mg^{2+} entry, whereas, silencing of MagT1 only partially decreased Mg^{2+} entry in naïve Mφ (Supplementary Fig. 1N), suggesting that this Mg^{2+} entry channel differs from the currently known Mg^{2+} channels.

Lipopolysaccharide (LPS) or IFN-γ can induce M1 polarization; meanwhile, M2 polarization is achieved by the addition of IL-4[1,37–39]. Treatment of naïve Mφ with LPS or IL-4 increases intracellular [Mg^{2+}] (Supplementary Fig. 2A, B). To further evaluate this, naïve Mφ were polarized with IFN-γ (20 ng/ml) or IL-4 (20 ng/ml) for 24 h, and the expression of Mg^{2+} entry channels was evaluated. Immunoblot analysis of Mg^{2+} channels and transporters showed expression of TRPM6, TRPM7, and MagT1 was observed in naïve Mφ an increase in MagT1 expression, but not that of TRPM6/7, was observed in IFNγ-induced M1 macrophages. Similarly, a distinct elevated expression of TRPM7 was observed in IL4-induced M2 macrophages (Fig. 2P), showing an interesting distinction in the expression of individual Mg^{2+} entry channels between the two macrophage phenotypes.

Mg^{2+} influx in M1 macrophages occurs via a selective Mg2+ channel that modulates its polarization and maintains the M1 phenotype

Data presented above shows that distinct Mg^{2+} entry channels are present in naïve Mφ. To outline the signaling mechanism by which Mg^{2+} modulates the M1 effector function, we next characterized the Mg^{2+} entry channel critical for the M1 phenotype. Naïve macrophages were treated with IFNγ (20 ng/ml) for 24 h and M1-polarization was confirmed using flow cytometry. Increased CD80 and reduced CD206 signify M1 polarization (Fig. 3A)[40,41]. The analysis of intracellular Mg^{2+} levels showed a significant increase in Mg^{2+} levels in M1 cells compared with naïve Mφ (Fig. 3B, C). Evaluation of TRPM7 currents in M1 cells showed a decrease in TRPM7 channel activity compared with naïve Mφ (Fig. 3D, E). Next, an in vivo murine model of peritonitis was used, and wildtype mice were i.p. infected with *Klebsiella pneumoniae* (KPN) or PBS (CTRL) for 24 h before collection

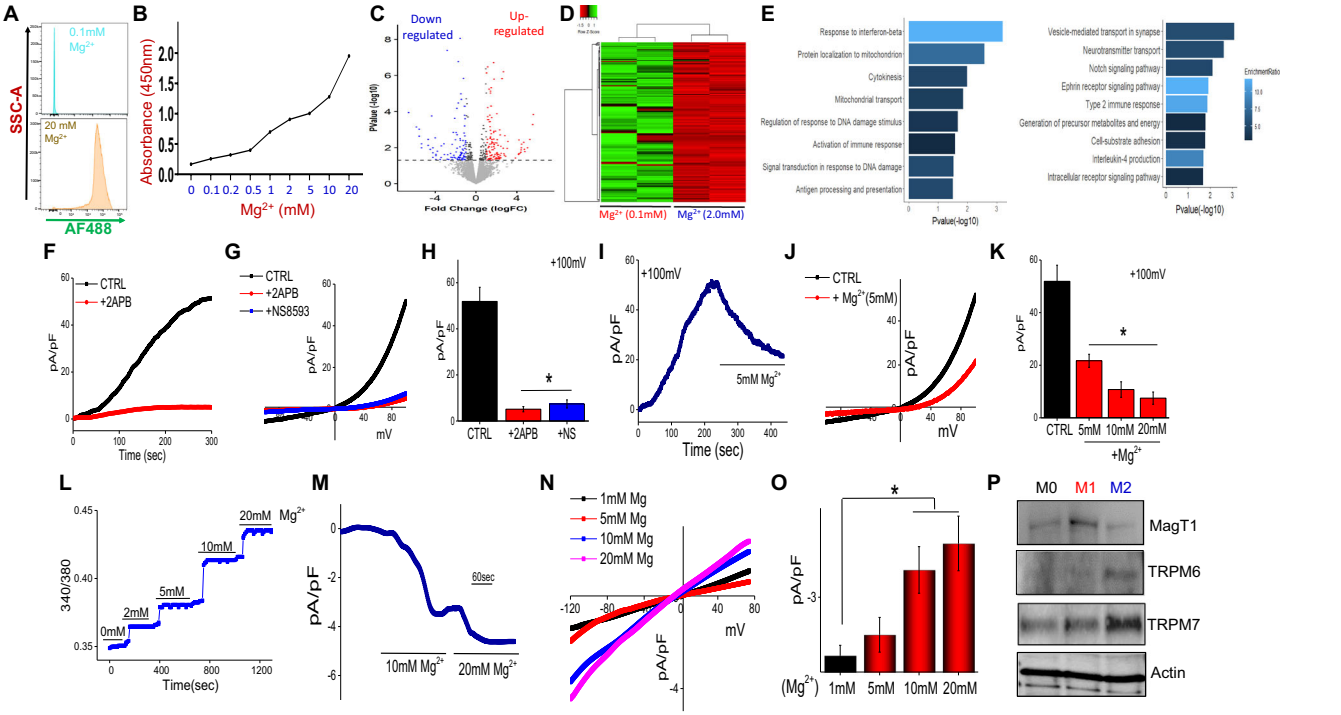

Fig. 2 | Characterization of Mg^{2+} entry channels in macrophage cells. A Flow cytometry proliferation analysis of naïve BMDM (Mφ) from WT mice (C57BL/6 J) at 24 h after treatment with 0.1 mM Mg^{2+} and 20 mM Mg^{2+}. Results from immunophenotyping experiment to evaluate cell proliferation with CFDA-SE. Data are represented as histograms of AlexaFluor488 expression (mean ± SD) of different treatments from three independent experiments. **B** Cell viability was performed in naïve Mφ cultured with different Mg^{2+} concentrations by BrdU colorimetric assay. Data shown are representative of three independent experiments with similar results. **C** Volcano plot showing changes in gene expression in primary Mφ cultured with 0.1 mM Mg^{2+} and 2.0 mM Mg^{2+}. **D** Heatmap showing genes that were increased in Mφ cultured at higher (2.0 mM) Mg^{2+} concentrations than cells growing in 0.1 mM Mg^{2+}. **E** Gene ontologies (GO) and pathway analysis showing an increase in biological pathways in Mφ cultured with 2.0 mM Mg^{2+} and at 0.1 mM Mg^{2+}. **F** Representative whole cell recording (n = 8-10) showing outward currents at +100 mV in control and 2APB treated (100 μM) Mφ cells are presented. **G** IV curves (acquired when currents reach peak) under various conditions (Bath application 100 μM 2APB, or 20 μM NS8593) as labeled in the figure, and quantitation of current density at +100 mV is shown in (**H**). **I–K** Bath application 5 mM Mg^{2+} inhibited TRPM7-like current. IV curves and quantitation of current density at +100 mV under various conditions (Bath application 5 mM Mg^{2+}, 10 mM Mg^{2+}, or 20 mM Mg^{2+}) as labeled in the figure. Data shown are representative of (8-12 individual patches). **L–O** Increasing external Mg^{2+} increases Mg^{2+} entry, as shown in analog plots of the fluorescence ratio (340/380). Bath application of 5-20 mM Mg^{2+} induced an inward current (holding at −120mV). IV curves (**N**) and quantitation (**O**) of current density at -120mV under various conditions as labeled in figure. indicate significance ($p < 0.05$). **P** Immunoblotting analysis showing the level of protein expression in wildtype mice naïve BMDM in comparison with activated M1 and M2 BMDM. Data shown are representative of three independent experiments with equivalent results.

of peritoneal macrophages for electrophysiological analysis. Again, TRPM7 currents in KPN-induced M1 cells showed a decrease in TRPM7 activity compared with PBS-treated macrophages (Supplementary Fig. 2C–E). In contrast, increasing external Mg^{2+} (20 mM) showed activation of a novel channel, which was significantly higher in M1 cells as compared with naïve Mφ, without any changes to its reverse potential (Fig. 3F, G). Moreover, silencing of MagT1 only partially decreased this Mg^{2+}-dependent channel activity (data not shown), suggesting that MagT1 is not the major Mg^{2+} entry channel in M1 cells.

We next evaluated the function of external Mg^{2+}, and as expected, low or removal of external Mg^{2+} leads to a decrease in the development/activation of the M1 phenotype. Flow cytometry assays were performed to evaluate the proliferation (with AlexaFluor488 beads) and for the development of the M1 phenotype. Notably, a significant decrease in M1 proliferation was observed in cells devoid of Mg^{2+}; whereas a high concentration of Mg^{2+} induced M1 proliferation (Fig. 3H). Moreover, flow cytometry further showed that a gradual increase of external Mg^{2+} increases the surface markers for M1 markers (CD80), suggesting that Mg^{2+} is critical for developing the M1 phenotype (Fig. 3I, J). Similarly, a significant increase in the release of pro-inflammatory cytokine (IL-6) was observed in the presence of high Mg^{2+} concentrations (Fig. 3K). Significantly, the addition of 2APB (50 μM for 6 hr) and SKF treatment (10 μM for 6 hr) decreased the release of pro-inflammatory cytokines (IL-6 and IL-1β) (Fig. 3L, M). However, increasing external, Mg^{2+} concentration (20 mM) was able to overcome 2APB/SKF-mediated inhibition of the pro-inflammatory cytokines (Fig. 3L, M). Consistent with these results, increasing external Mg^{2+} concentration also leads to an increase in NFκB phosphorylation and iNOS expression, suggesting a positive activation by Mg^{2+} in regulating the M1 phenotype (Fig. 3N). Together the data presented suggest that Mg^{2+} influx via an unknown Mg^{2+}-dependent channel is essential for M1 survival, as well as for the activation of downstream signaling factors that modulate cytokine releases and in the development of the activated M1 phenotype.

M2 phenotype polarization is mediated by TRPM7 activation

Activation of the M1 phenotype is critical for inhibiting infections; however, after the resolution of the infection process, these macrophages are transformed into the anti-inflammatory M2 phenotype. Thus, we next investigated if, Mg^{2+} would also have similar effects on the M2 phenotype. Naïve macrophages from wildtype mice were polarized by treating with IL-4 (20 ng/ml) for 24 h. Flow cytometry was utilized to confirm M2-polarization by detection of the M2 surface marker, $CD206^{+}$ (Fig. 4A). IL-4 caused an increase in intracellular Mg^{2+} levels in M2 Mφ (Supplementary Fig. 2B), and the release of anti-inflammatory cytokines was observed in M2 cells grown in Mg^{2+} (1 mM) (Fig. 4B). In contrast, pretreatment with high concentrations of Mg^{2+} (5 mM) decreased the release of anti-inflammatory cytokine IL1RA (Fig. 4B). Moreover, 1 mM Mg^{2+} was

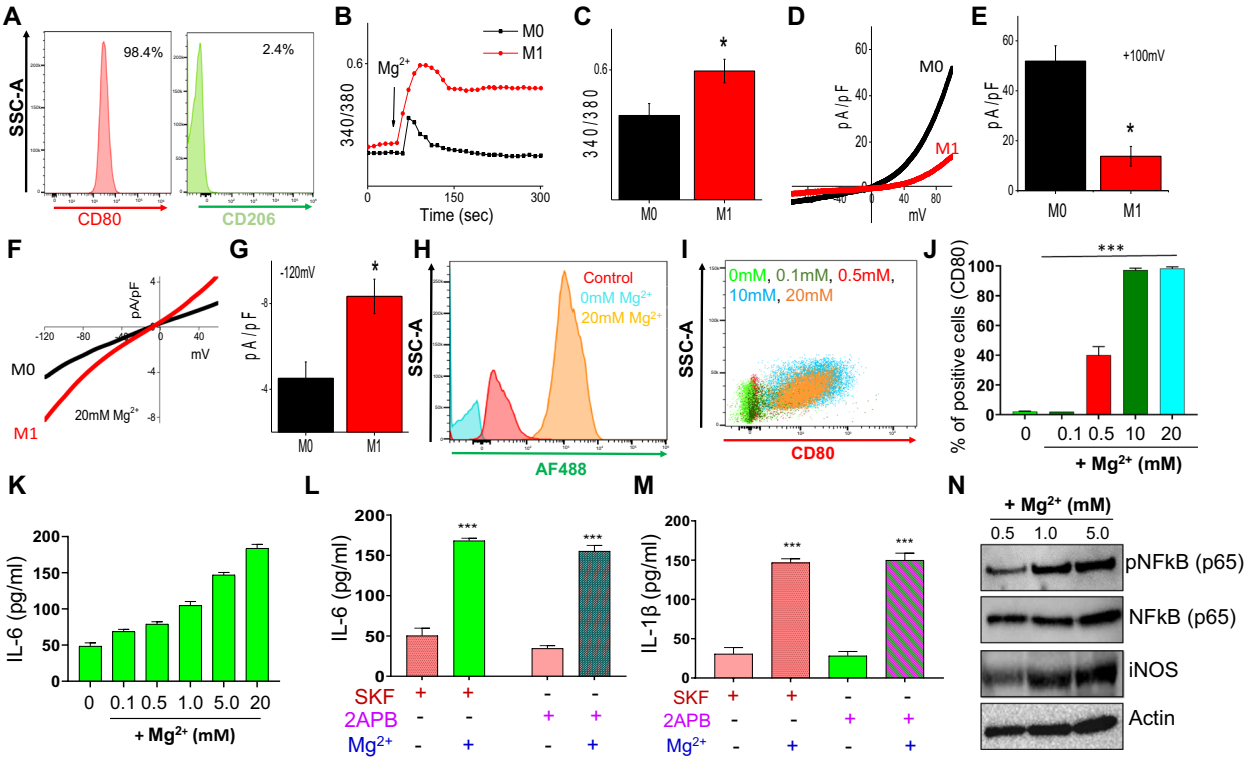

Fig. 3 | Higher Mg^{2+} entry is critical for the development of the M1 phenotype. **A** Flow cytometer analysis on WT mice cells was performed to measure the levels of surface markers to demonstrate the efficacy of cell polarization. Data show a high $CD80^+$ M1 marker and low $CD206^+$ M2 marker to illustrate successful M1 polarization when naïve M0 cells are treated with IFN-γ (20 ng/ml) for 24 h. Data shown are representative of three independent experiments with comparable results. **B** Mg^{2+} imaging was performed using Mag-Fura in M0 and M1 cells. Bath application of 20 mM Mg^{2+} induces Mg^{2+} influx, and analog plots of the fluorescence ratio (340/380 from 50-60 cells) are shown. **C** Quantification (mean ± SE) of intracellular Mg^{2+} concentration. *indicate significance ($p < 0.05$). IV curves of TRPM7 current in M0 and M1 cells and quantitation of current density at +100 mV (mean ± SD of 6 experiments) are shown in (**D**) and (**E**). **F**, **G** IV curves of Mg^{2+} entry current in M0, M1 cells and quantitation of current density at -120mV (mean ± SD of 6 experiments) are represented in this figure. **H** Proliferation analysis by CFDA-SE Alexa Fluor488 fluorescence on M1 activated wild type mice BMDM treated with media containing 0 mM Mg^{2+} and 20 mM Mg^{2+} versus control to show the impact of no magnesium on M1 macrophage proliferation. Data shown in histograms are representative of three independent experiments with similar results. **I** Flow cytometer analysis on M1 activated wild type mice BMDM treated with several Mg^{2+} concentrations (0 mM, 0.1 mM, 0.5 mM, 10 mM, and 20 mM) for 24 hr to show how magnesium is relevant for macrophage polarization, increasing $CD80^+$ M1 marker expression. Data shown are representative of three independent experiments with similar results. Bar graphs depict average ± SD for relative values in (**J**), $***p \le 0.001$, (Student's *t*-test). **K** Activated BMDM M1 cells cultured in 6 wells plate (2×10^6 cells/well) and treated with 0 mM, 0.1 mM, 0.5 mM, 1 mM, 2 mM and 5 mM Mg^{2+} for 24 hr. The concentration of pro-inflammatory cytokines IL-6 released in the media was performed by ELISA and bar graphs depict average ± SD for relative values (n = 3), $***p \le 0.001$ (Student's *t*-test). **L**, **M** Activated BMDM M1 cells cultured in 6 wells plate (2×10^6 cells/well) and treated with 2APB (10 μM) plus 2APB + 20 mM Mg^{2+} and 2APB + 20 mM Ca^{2+}; SKF (10 μM) plus SKF + 20 mM Mg^{2+} and SKF + 20 mM Ca^{2+} overnight. The concentration of pro-inflammatory cytokines (IL-6 and IL1-β) released in the media was performed by ELISA. Data shown are representative of three independent experiments with similar results. Bar graphs depict average ± SD for relative values, $***p \le 0.001$ (Student's *t*-test). **N** Immunoblotting analysis showing the level of expression of pNFκB, NFκB, iNOS, and β-actin in wildtype mice M1 activated BMDM with increasing Mg^{2+} concentrations. Data shown are representative of three independent experiments with equivalent results.

sufficient to increase M2 polarization; whereas, lower (0 mM, 0.1 mM) or higher (10 mM and 20 mM) Mg^{2+} levels decreased the M2 phenotype (as shown by a decrease in ($CD206^+$) expression) (Fig.4C, D). Nonspecific channel blockers such as 2APB (50 μM for 6 h) and SKF (10 μM for 6 h) showed a significantly lower release of anti-inflammatory cytokines (IL1RA and IL10) (Fig. 4E, F). Interestingly, high concentrations of Mg^{2+} (20 mM) failed to show any increase in the release of the same cytokines (Fig. 4E, F). These data are in contrast with the data observed in M1 cells and suggest that perhaps higher Mg^{2+} levels can inhibit the development of the M2 phenotype.

To establish the identity of the Mg^{2+} entry channels that modulate the M2 phenotype, we again evaluated the electrophysiological properties of the channel. Similar to naïve Mφ, decreasing intracellular Mg^{2+} led to the development of an TRPM7-like outward rectifying current, which reversed close to 0 mV in M1 cells (Fig. 4G, H). In contrast, a significant decrease in the current properties of the novel Mg^{2+}-dependent channel was observed (Fig. 4I–K). Naïve Mφ showed a linear Mg^{2+}-evoked current, and increasing external Mg^{2+} (20 mM) led to an increase in the Mg^{2+} current, which was not observed in M2 cells (Fig. 4I-K). To further confirm the role of these different Mg^{2+} channels on M2 phenotype polarization, immunoblotting was performed on M2 cell lysates. Importantly, the expression of Arginase 1 and pSTAT6, the classical activation markers of M2 cells, was highest when cells were incubated in 1 mM external Mg^{2+} (Fig. 4L). Furthermore, either decreasing (0.5 mM) or increasing Mg^{2+} (5 mM) concentration leads to a decrease in the phosphorylation of STAT6 and the expression of Arginase1 (Fig. 4L). Consistent with these results, TRPM7 expression was also increased at 1 mM external Mg^{2+} but decreased drastically when increasing Mg^{2+} (5 mM) concentration (Fig. 4L). Importantly, a functional angiogenesis assay was also performed on the supernatants of M2 phenotype cells when treated with varying concentrations of Mg^{2+}. Interestingly, a significant increase in the release of VEGF was directly related to Mg^{2+} concentrations in the range of 1-2 mM, as either decreasing or increasing Mg^{2+} levels further inhibited M2 function (Fig. 4M). Also, a significant increase in cell proliferation of M2 cells[42,43] was observed by increasing the Mg^{2+} concentrations (Supplementary Fig. 2F, G). Interestingly, modulating external Mg^{2+} levels (independent of cytokine stimulation), lead to the polarization

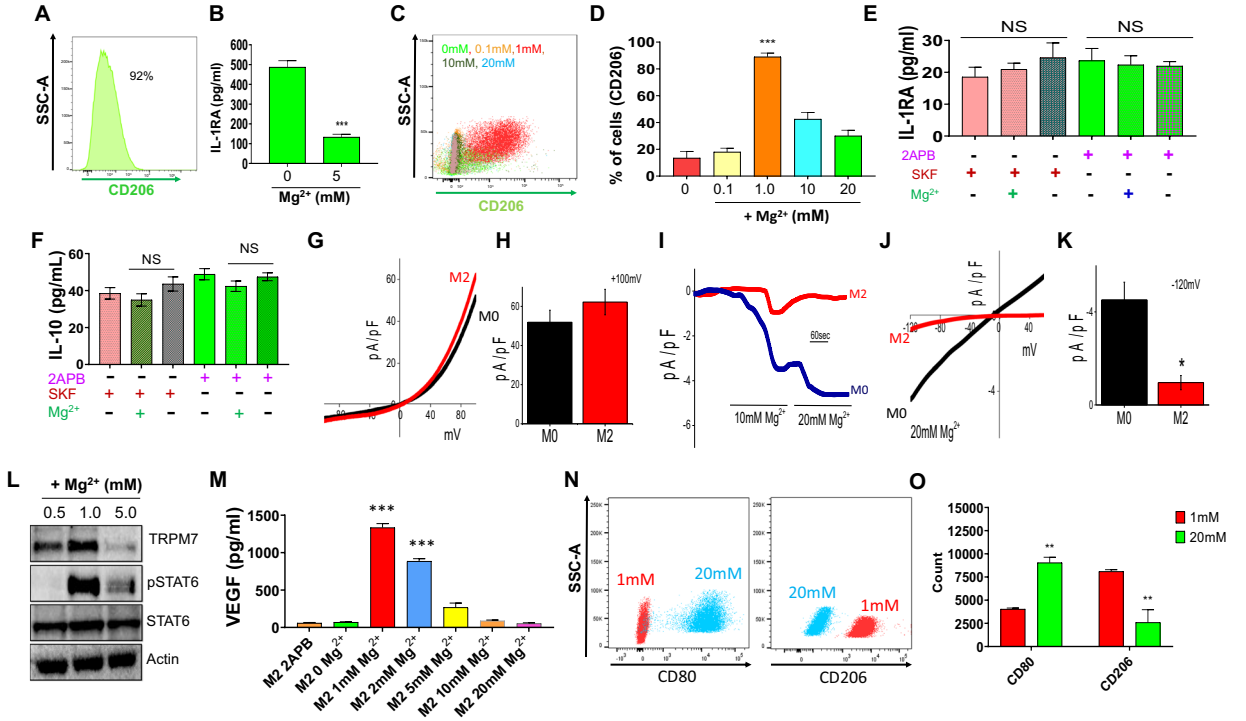

Fig. 4 | Mg^{2+} entry via TRPM7 channels facilitates the M2 phenotype. A Flow cytometer analysis on WT mice cells was performed to measure the levels of surface markers to demonstrate the efficacy of cell polarization. Data show a high $CD206^{+}$ M2 marker and low $CD80^{+}$ M1 marker to illustrate successful M2 polarization when naïve M0 cells are treated with IL-4 (20 ng/ml) for 24 h. Data shown are representative of three independent experiments with similar results. **B** Activated BMDM M1 cells cultured in 6 wells plate (2×10^6 cells/well) and treated with 1 mM and 5 mM Mg^{2+} and Ca^{2+} for 24 hr. The concentration of anti-inflammatory cytokine IL-1RA released in the media was performed by ELISA. Data shown are representative of three independent experiments with similar results. Bar graphs depict average ± SD for relative values, $^{***}p \le 0.001$ (Student's *t*-test). **C**, **D** Flow cytometer analysis on M1 activated wild type mice BMDM treated with several Mg^{2+} concentrations (0 mM, 0.1 mM, 0.5 mM, 5 mM, 10 mM and 20 mM) for 24 hr to show how Mg^{2+} is relevant for macrophage polarization, increasing CD80 + M1 marker expression. Data shown are representative of three independent experiments with similar results. Bar graphs depict average ± SD for relative values, $^{***}p \le 0.001$ (Student's *t*-test). **E**, **F** Activated BMDM M2 cells cultured in 6 wells plate (2×10^6 cells/well) and treated with 2APB (10 μM) plus 2APB + 20 mM Mg^{2+} and 2APB + 20 mM Ca^{2+}; SKF (10 μM) plus SKF + 20 mM Mg^{2+} and SKF + 20 mM Ca^{2+} overnight. The concentration of anti-inflammatory cytokines (IL-10 and IL-1RA) released in the media was performed by ELISA. Data shown are representative of three independent experiments with similar results. Bar graphs depict average ± SD for relative values, NS = non-significant (Student's *t*-test). **G** IV curves of TRPM7 current in M0, M2 cells and quantitation of current density at +100 mV (mean ± SD of 6 experiments) is shown in (**H**). Bath application 10 mM Mg^{2+}, 20 mM Mg^{2+} induced inward current (holding at -120mV) are shown in (**I**). IV curves (**J**) and quantitation of current density at −120mV (**K**) in M0, M2 cells, as labeled in the figure. **L** Immunoblotting analysis showing the level of expression of TRPM7, pSTAT6, STAT6, and β-actin in wildtype mice M2 activated BMDM with increasing Mg^{2+} concentrations. Data shown are representative of three independent experiments with similar results. **M** Elisa quantification for VEGF in supernatants of M2 activated BMDM with 2APB treatment (10 μM overnight) and increasing Mg^{2+} concentrations. Data shown are representative of three independent experiments. Bar graphs depict average ±SD for relative values, $^{***}p \le 0.001$ (Student's *t*-test). **N**, **O** Flow cytometer analysis on naïve BMDM (Mφ) with supplemented with 1 mM and 20 mM Mg^{2+} concentrations for 24 hr, showing the presence of M1 (CD 80) and M2 (CD 206) markers respectively. Bar graphs depict average ±SD for relative values, $^{**}p \le 0.005$ (Student's *t*-test).

of naïve Mφ. Higher Mg^{2+} levels (20 mM), promoted the development of M1 phenotype, along with a suppression of M2 cells (Fig. 4N, O). In contrast, supplementation of 1 mM Mg^{2+} to naïve Mφ led to an increase in M2 markers (Fig. 4 N, O), suggesting that external Mg^{2+} levels are sufficient to modulate macrophage polarization.

Differential Mg^{2+} entry is critical for maintaining the mitochondrial bioenergetics in M1/M2 phenotypes

Metabolism has been suggested as a key regulator for immune cell (M1/M2) differentiation and its activation[44,45]. Importantly, both glycolysis and oxidative phosphorylation have been shown to modulate macrophage polarization, but factors that could alter oxidative phosphorylation are not known. Interestingly, Mg^{2+} has a stimulatory effect on several mitochondrial enzymes, thereby can significantly impact the metabolic state of immune cells. Thus, we evaluated mitochondrial Mg^{2+} levels in various macrophage phenotypes. Importantly, a significant difference in intracellular mitochondrial Mg^{2+} ($_{m}Mg^{2+}$) levels was observed between naïve, M1, and M2 macrophages. Naïve macrophages from WT mice exhibited a higher level of basal $_{m}Mg^{2+}$ release upon FCCP uncoupling than the M1 polarized macrophages. Conversely, the M2 macrophages exhibited a higher intrinsic $_{m}Mg^{2+}$, restored to the levels of naïve macrophages, that would drive a lowering of mitochondrial metabolism and ATP synthesis (Fig. 5A, B).

In contrast, higher mitochondrial Mg^{2+} levels were observed in naïve and M2 phenotypes, suggesting that changes in mitochondrial Mg^{2+} levels might be essential for macrophage polarization. Importantly, with 20 mM Mg^{2+} for 1 hour, we observed an inverse effect of Mg^{2+} retention in the mitochondria. While the M1 macrophages retained similar levels of basal mMg^{2+} to the absence of extracellular Mg^{2+}, M2 macrophages exhibited a reduced level of basal Mg^{2+} than M1 macrophages (Fig. 5C, D).

We further evaluated the oxygen consumption rate (OCR), which is a readout for mitochondrial bioenergetics in these different conditions. Interestingly, we observed that loss of external Mg^{2+} exhibited lower OCR, and levels of basal, maximal, and proton leak were inhibited in all the macrophage phenotypes (Fig. 5E–J). However, increasing Mg^{2+} levels (20 mM) showed a significant increase in both basal and maximal respiration in M1 cells (Supplementary Fig. 2H), suggesting that high Mg^{2+}

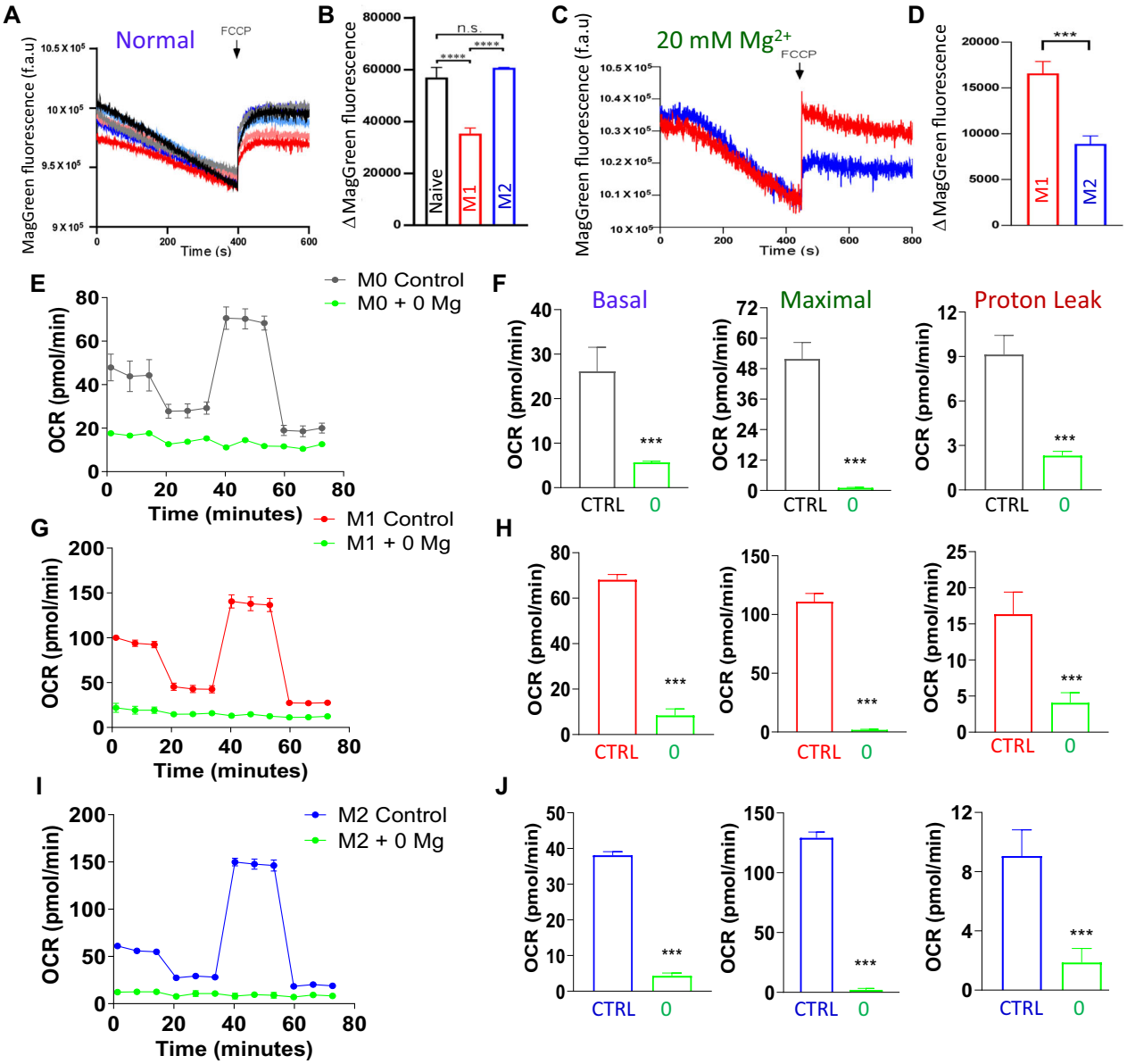

Fig. 5 | Mitochondrial function is dependent on Mg^{2+} entry in macrophage cells. **A** Spectrofluorimetric traces depicting permeabilized macrophages (Naïve, M1, M2) exposed to FCCP at the indicated time point to assess basal mMg^{2+}. **B** Quantification of basal mMg^{2+} in permeabilized macrophages. **C** Spectrofluorimetric traces representing permeabilized macrophages (M1, M2) in the presence of 20 mM Mg^{2+} for 1 h exposed to FCCP at the indicated time point to assess basal mMg^{2+}. **D** Quantification of basal mMg^{2+} in permeabilized macrophages in the presence of Mg^{2+}. **E**, **G**, **I** Oxygen Consumption Rate (OCR) was analyzed in macrophages isolated from WT with and without Mg^{2+} for 1 hour for M0, M1, and M2 phenotypes. N = 3 performed in duplicate. **F**, **H**, **J** Basal, maximal respiration, and proton leak analysis of macrophages isolated from WT with and without Mg^{2+} for 1 hour. Mean ± SEM, n = 3, $***p < 0.001$.

concentration is perhaps needed to maintain the M1 phenotype. In contrast, M2 cells failed to show any increase in the maximal respiration and the basal respiration levels at higher Mg^{2+} levels (20 mM) (Supplementary Fig. 2H). Together these results suggest that there is a tight regulation of Mg^{2+} entry in the mitochondria that is critical for regulating the metabolic programming and phenotypic plasticity in macrophage cells.

TRPM7 is sufficient for the development of the M2 phenotype and tumor growth without altering the M1 phenotype

Based on the data presented above, we assessed the physiological effect of TRPM7 on M2 polarization. Naïve Mφ (M0) or IFNγ-treated (M1) or IL-4-treated M2 cells were either transfected with non-targeting siRNA (SiC, for control) or TRPM7siRNA (siTRPM7) to evaluate its role in the development of the M2 phenotypes. Immunoblot analysis showed a decrease in TRPM7 protein in all macrophage cells (Fig. 6A). Importantly, loss of TRPM7 in M2 cells displayed low expression of the classical M2 protein marker "Arginase 1" when compared with control siRNA treated cells (Fig. 6A), Electrophysiological analysis further showed a decrease in TRPM7 currents in M2 cells that express siTRPM7, without altering the previously unidentified Mg^{2+}-dependent channel function in M1 cells (Fig. 6B, C). Elisa assay further showed a significant decrease in the release of anti-inflammatory cytokines from M2 cells without affecting the pro-inflammatory M1 cytokines (Fig. 6D, E). Notably, silencing of TRPM7, but not MagT1, significantly decreased VGEF levels (Fig. 6F) as well as mitochondrial function (OCR) was also inhibited upon TRPM7 silencing in M2 cells (Fig. 6G, H).

We further investigated the importance of the activation TRPM7 channel in macrophage polarization by treating the cells with a known TRPM7 activator (Naltriben)[46]. Naïve macrophage cells treated with Naltriben (NTB) (20 μM) for 24 h showed a clear increase in TRPM7

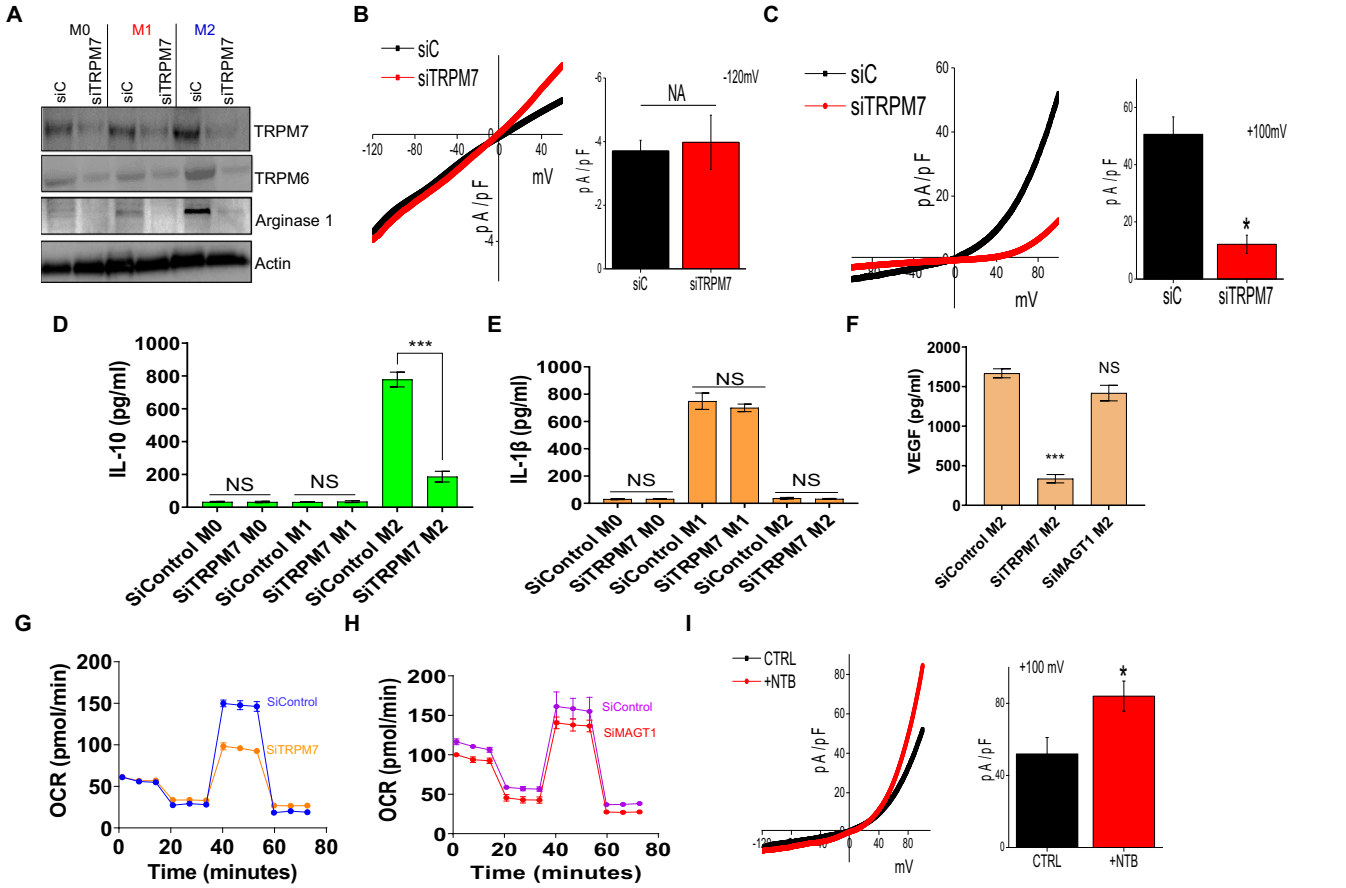

Fig. 6 | TRPM7 channel is important for the M2 phenotype. A Western blots showing expression of various proteins in silenced TRPM7 in naïve M0 plus activated BMDM M1 and M2 cells cultured in 6 wells plate (2×10^6 cells/well). **B**, **C** IV curves of Mg^{2+} entry currents in control, siTRPM7 naïve M0 cells, and quantitation of current density at -120mV is shown as bar graph. TRPM7 current is in control, and siTRPM7 cells (**C**) are quantitated at current density at +100 mV. **D**, **E** The concentration of pro and anti-inflammatory cytokines (IL-1β and IL-10, respectively) released in the media. Data shown are representative of three independent experiments with similar results. Bar graphs depict average ± SD for relative values, $***p \le 0.001$, NS = non-significant (Student's *t*-test). **F** Quantification for VEGF in supernatants of M2-activated BMDM with siTrpm7 and siMagt1 in comparison with siControl. Data shown are representative of three independent experiments. Bar graphs depict average ±SD for relative values, NS = non-significant, $***p \le 0.001$ (Student's *t*-test). **G**, **H** Oxygen Consumption Rate (OCR) was analyzed in M2 macrophages with control siRNA or MagT1 or TRPM7 siRNA, respectively. N = 3 performed in duplicate. **I** IV curves of TRPM7 currents (acquired when currents reach peak) in control and 50 μM NTB groups as labeled in the figure and are shown. The quantitation of current density at -+100 mV is shown as a bar graph. $*p \le 0.01$.

channel activity (Fig. 6I). Flow cytometry was also performed on the naïve cells treated with different concentrations of NTB, interestingly two of the major M2 phenotype markers, EGR2 and arginase, were increased in the presence of NTB, which was similar as observed with IL-4 (Fig. 7A, B; Supplementary Fig. 2I). Similarly, the levels of M2 cytokines, IL-1Ra, and IL-10 were also increased by the treatment with NTB (Fig. 7C; Supplementary Fig. 2J). Consistent with these results, a significant increase in VEGF levels was observed in cells treated with NTB (Fig. 7D). Furthermore, increasing NTB concentration also led to a constant increase in the expression of arginase (Fig. 7E), clearly showing that the activation of the TRPM7 channel by NTB plays a vital role in M2 phenotype polarization and thus critical for immune functions. Finally, mice treated with naltriben (TRPM7 agonist), promoted tumor growth (Fig. 7F). Together the data presented here, suggest that macrophage polarization is dependent on Mg^{2+} entry, where high levels of Mg^{2+} influx through an uncharacterized high-affinity Mg^{2+} influx channel drive the classically activated M1 phenotype and increase pro-inflammatory cytokines. In contrast, the alternatively activated M2 phenotype requires a low threshold Mg^{2+} entry channel, which is mediated by TRPM7 activation that leads to anti-inflammatory phenotype and tumor induction. Furthermore, activation of TRPM7 (via Naltriben) is sufficient to induce M2 phenotype and promote macrophage plasticity and tumor progression (Fig. 7G).

Discussion

In the presence of pathogens, macrophages polarize into the classical M1 phenotype, whereas the alternative M2 phenotype is essential for the resolution of inflammation and tissue repair. Similarly, macrophages can either promote or prevent tumor development. Thus, understanding factors that modulate macrophage polarization could lead to novel strategies for their reprogramming as a potential means to prevent infections, treat inflammatory diseases, and prevent cancer. In this study, we have demonstrated that Mg^{2+} is essential for regulating macrophage function, and sequestering external Mg^{2+} levels inhibited their proliferation and induced cell death. Importantly, reprogramming of naïve Mφ toward the M1 and M2 phenotype was also dependent on Mg^{2+} entry and inhibiting Mg^{2+} entry, decreased both pro- and anti-inflammatory cytokines. Moreover, we have identified distinct Mg^{2+} channels that increase Mg^{2+} entry in M1 and M2 phenotypes that are needed for maintaining their functions. Although previous studies have identified different modulators that induce transcriptional regulations along with metabolic reprogramming as the key factors that regulate macrophage polarization[47], events that are upstream of mitochondrial bioenergetics/transcription regulation have not been identified.

Importantly Mg^{2+} entry was vital for maintaining critical macrophage functions, and naive macrophages express several of the known Mg^{2+} entry channels. Increasing Mg^{2+} levels increased cell proliferation in naïve macrophages; however, it also inhibited TRPM7 currents, suggesting that

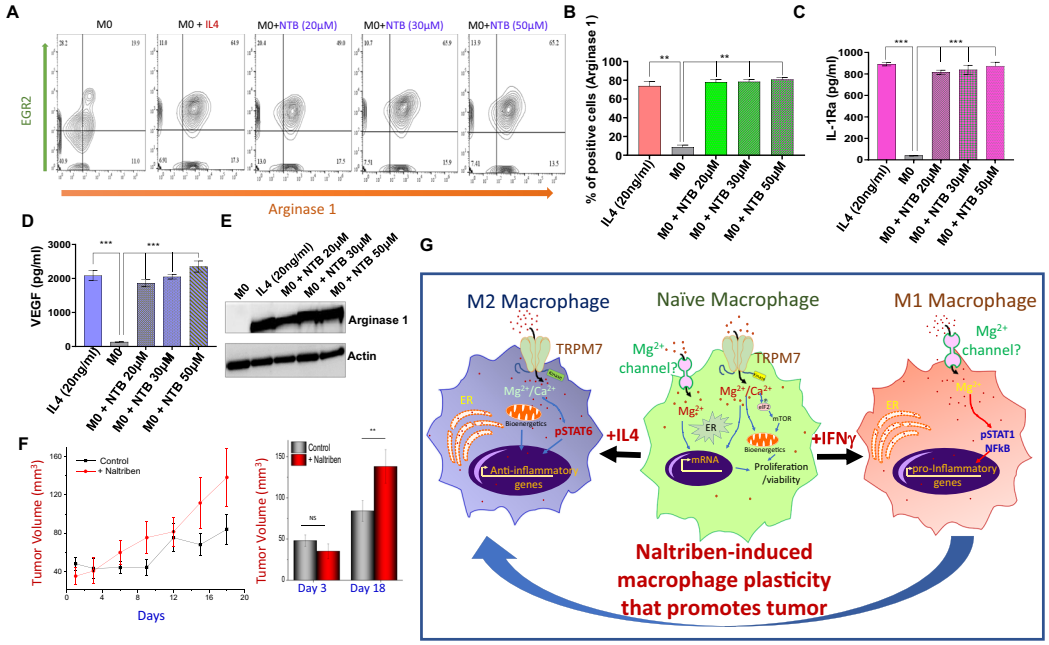

Fig. 7 | Naltriben-induced activation of TRPM7 channel promote the M2 phenotype and tumor progression. A–C Flow cytometer analysis on M0 activated wild type mice BMDM treated with IL4 or Naltriben-treated cells at different concentrations (20 μM, 30 μM, 50 μM) for 24 hr to show how TRPM7 activation is relevant for macrophage polarization, increasing expression of Arginase 1 (**B**). Data shown are representative of three independent experiments with similar results. Bar graphs depict average ± SD for relative values, $^{**}p \le 0.01$, (Student's *t*-test). **C** Naïve M0 cells cultured in 6 wells plate (2×10^6 cells/well) and treated with IL-4 (20 ng/ml) and Naltriben treatment (20 μM, 30 μM and 50 μM) for 24 h. The concentration of anti-inflammatory cytokines (IL-10 and IL-1RA) released in the media was performed by ELISA. Data shown are representative of three independent experiments with similar results. Bar graphs depict average ± SD for relative values, $^{***}p \le 0.001$ (Student's *t*-test). **D** Elisa quantification for VEGF in supernatants of naïve (M0) BMDM with and without IL-4 treatment (20 ng/ml) and Naltriben treatment (20 μM, 30 μM and 50 μM) for 24 h. Data shown are representative of three independent experiments. Bar graphs depict average ±SD for relative values, $^{**}p \le 0.01$, $^{***}p \le 0.001$ (Student's *t*-test). **E** Immunoblotting analysis showing the level of expression of arginase and β-actin of wildtype mice naïve M0 with and without IL-4 (20 ng/ml) and Naltriben treatment (20 μM, 30 μM and 50 μM) for 24 h. The data shown are representative of three independent experiments with similar results. **F** Tumor volumes (average ±SE) under various conditions (n = 6). **G** The schematic overview of macrophage polarization, where Mg^{2+} influx drives macrophage phenotype transformation. M1:classically activated and pro-inflammatory cytokines release (IL-6, IL1β, TNFα) is regulated by an uncharacterized Mg^{2+} influx channel. In contrast activation and anti-inflammatory cytokine release (IL-10, IL-1rn, and IL1RII) are controlled by TRPM7, and it can be induced by Naltriben to promote plasticity.

additional Mg^{2+} channels could be essential in modulating their function. Previous studies have identified that TRPM7 is vital for macrophage function; however, this function was linked to its ability to bring in Ca^{2+}, which could suggest that perhaps TRPM7 modulates the basal function in naïve macrophages. Interestingly, similar to previous findings[33], TRPM7 exhibited a small inward current, but higher outward currents in macrophage cells, suggesting that higher levels of Mg^{2+} entry could not be through TRPM7 channels. Interestingly, Mg^{2+}-induced Mg^{2+} influx in thymocytes that were obtained from *Trpm7*$^{-/-}$ mice were insensitive to the deletion of TRPM7, indicating that additional Mg^{2+} influx channels are functional in immune cells[33]. To further evaluate the identity of this critical Mg^{2+}-induced Mg^{2+} entry channel, we evaluated the expression and functional properties of this elusive channel. Our results show that increasing external Mg^{2+} leads to a dose-dependent increase in Mg^{2+} entry that was critical for the development of the M1 phenotype. This uncharacterized channel was not mediated via MagT1, Slc41a/b/c, or Tmem63b but had some similar current features (linear, similar reverse potential), but few distinctive channel features were also noted (selectivity towards Mg^{2+}, not blocked by Gd^{3+}, activated by external Mg^{2+}). Although the molecular identity of this channel is not yet known, we did rule out that none of the recently identified Mg^{2+} channels are indeed the Mg^{2+}-induced Mg^{2+} entry channel, and more research is needed to identify this important channel. Interestingly, an increase in plasma Mg^{2+} concentration was observed in leukocytes during an acute asthma attack[48], which is mediated via the M1 pro-inflammatory phenotype. These results support our findings that higher external Mg^{2+} levels induce an Mg^{2+}-induced Mg^{2+} entry channel that modulates the pro-inflammatory M1 macrophages. Interestingly silencing of MagT1 only partially decreases the Mg^{2+}-induced Mg^{2+} entry channel. MagT1 is expressed both in the plasma membrane as well as in the endoplasmic reticulum, where plasma membrane MagT1 could contribute to Mg^{2+} entry or assist the unknown Mg^{2+}-induced Mg^{2+} entry channel. Nonetheless, our data showed that the Mg^{2+}-induced Mg^{2+} entry channel was critical for the development of the M1 phenotype a, which could prevent infection and cancer progression.

Classically activated M1 macrophages have long been known to be induced by IFNγ alone or in concert with microbial stimuli (e.g., LPS). Interestingly, the addition of LPS or IFNγ led to an increase in intracellular Mg^{2+} levels, suggesting that Mg^{2+} could provide the initial trigger needed for their polarization and development into the M1 phenotype. Importantly, a decrease in extracellular Mg^{2+} levels led to a decrease in M1 surface markers and increasing Mg^{2+} levels restored the M1 phenotype. Nude mice that lack T and B cells, were used for our experimentation as we used human tumor cells, which can only grow when T cells are absent. Nonetheless, nude mice on an Mg^{2+}-deficient diet had decreased M1 cells and showed higher tumor volume, further strengthening the notion that Mg^{2+} levels dictate M1 polarization which is important for inhibiting tumor progression, particularly when T and B cells are absent. However, it cannot be excluded that the phenotypes observed in this study might be absent or even reversed in immunocompetent mice and more research is needed to evaluate this further. Importantly, macrophage polarization is a highly plastic and dynamic process, which could be easily modulated by Mg^{2+} entry. Notably, one of the important discoveries indicated here is that our results provide the spatial and temporal resolution that dictates these two opposing events. Although both M1 and M2 cells require Mg^{2+} entry for their function, they

both have different Mg^{2+} thresholds, which are regulated by distinct Mg^{2+} entry channels. M1 cells require high Mg^{2+} levels, which can only be provided through the Mg^{2+}-induced Mg^{2+} entry channel. Increasing extracellular Mg^{2+} was critical for resolving 2APB or SKF-mediated inhibition, which suggests that it can even override the Ca^{2+}-dependent process essential for immune activation. In contrast, M2 cells had a decreased Mg^{2+} threshold and needed lower Mg^{2+} levels, which are regulated by TRPM7 channels. These results are in contrast with a recent finding which showed that higher external Mg^{2+} was important for bone growth but decreased M1-like phenotype[36]. However, these results were generated using THP1 cell lines, which differ greatly from primary macrophages. In addition, it was suggested that TRPM7 was critical for these functions, which is inhibited by higher external Mg^{2+} [23,49], and thereby could not contribute to these functions.

One of the fundamental questions is how low Mg^{2+} entry from TRPM7 modulates the M2 phenotype. Our data shows that it activates the phosphorylation of STAT6, and increasing external Mg^{2+} that inactivates TRPM7 channels had a negative effect on STAT6 phosphorylation. Interestingly, TRPM7 also has a kinase domain, and it is possible that it can directly phosphorylate STAT6. In addition, the cleaved TRPM7 kinase fragments have also been shown to translocate to the nucleus and phosphorylate histones that modulate gene expression[50], which can also contribute to tumor development. Mg^{2+} entry through TRPM7 also regulated oxidative phosphorylation; therefore, an alternative explanation could be that M2 macrophages display enhanced mitochondrial oxidative phosphorylation in comparison to M1 macrophages[36,51]. Mg^{2+} levels have been shown to modulate mitochondrial function, and it is responsible for ion channels such as voltage-dependent Ca^{2+} channels and K^{+} channels[19,52]. Our data support that decreasing Mg^{2+} levels in M2 cells, but not in M1 cells, decreased oxidative phosphorylation. Importantly, a decrease in the expression of classical M2 markers and M2 cytokines was also decreased upon the downregulation of TRPM7. Interestingly, Mg^{2+}- a deficient diet promoted solid tumor growth, which was blocked by the inhibition of TRPM7, but increased via the activation of TRPM7. These results suggest that Mg^{2+} entry via TRPM7 is needed for maintaining the M2 phenotype without altering the M1 phenotype, and activation of TRPM7 by Naltriben was enough to induce M2 polarization and tumor development. In conclusion, we provide evidence that distinct Mg^{2+} channels and transporters are present in these macrophage phenotypes, and exploiting their unique characteristics could be critical for macrophage transformation.

Methods

Mice, primary cells, reagents, silencing of Magt1 and Trpm7, and Naltriben mesylate treatment

For the primary cells, C57BL/6 mice (6 weeks old, male) were used, and bone marrow-derived macrophages (BMDMs) were isolated from the femurs of mice. Femurs were flushed out with PBS using a sterile needle, then cultivated in a DMEM medium (Life Technologies, Carlsbad, CA, USA) containing L929 conditioned media. After 5 days, fully differentiated BMDMs formed on the culture plates' bottom. The isolated macrophage cells were then incubated at 37 °C in a DMEM medium supplemented with 10% FBS and 1% penicillin/streptomycin solution[53,54]. For silencing experiments, respective *Magt1* siRNA (ThermoFisher, Assay ID: 183726) and *Trpm7* siRNA (ThermoFisher, Assay ID:181935) were used, the transfection was performed with Lipofectamine® RNAi Reagent following the manufacturer's protocol. Cells were seeded to be 70% confluent, and the Lipofectamine 2000 reagent was diluted in an optimal concentration (ThermoFisher, LMRNA015) 25pmol per well in a 6-well dish) in Opti-MEM medium (Gibco, Dublin, Ireland). Lipofectamine was added to the diluted siRNA in a 1:1 ratio and incubated for 5 minutes at room temperature. The complex was then layered on the cells for 5 hours, followed by adding fresh media and used for individual experiments. For the experiments utilizing differential [Mg^{2+}] and [Ca^{2+}], HBSS (Hank's Balanced Salt Solution without calcium chloride, magnesium chloride, and magnesium sulfate, Gibco) was used with Ca^{2+} and Mg^{2+} added accordingly. Naltriben mesylate (Tocris, Minneapolis, MN, USA) treatment was performed on isolated naïve BMDM cells (2×10^6 cells per well) from WT mice at different concentrations (20 μM, 30 μM and 50 μM per well) in a 6 well dish for 24 h. Animal studies adhered to the international guidelines on animal welfare following the National Institute of Health Guide for the Care and Use of Laboratory Animals and complied with the ARRIVE guidelines and the 2013 AVMA euthanasia guidelines. All studies were approved by UT Health San Antonio (UT Health SA) Institutional Animal Care and Use Committee. Mg^{2+} and tumor studies were carried out in six- to eight-week-old female athymic nude mice given by Dr. Cara Gonzales (Department of Comprehensive Dentistry- UTHSCSA) under a laminar air-flow cabinet in pathogen-free conditions; both conditions were given under the skin of the conscious animal. Mice were kept in a 12 h light/dark schedule at controlled temperature and humidity with food and water ad libitum. Mice were acclimated for one week before the study initiation.

Magnesium deprivation diet and tumor studies

3×10^6 Cal-27 cells in saline solution were injected subcutaneously into the flank as described previously by us[55,56]. Animals were conscious during injection and no anesthesia was used in this section of the study. Mice were stratified into 2 experimental groups (n = 5 per group): A magnesium-deprived diet along with a respective control diet were purchased from Envigo, Madison WI, USA. Individual mice were acclimatized with respective diets for 3 days prior to the injection of the Cal27 cells, which was monitored for additional 28 days (when tumors achieved the expected size for selection). Mice were monitored daily for tumor growth using digital calipers and for cachexia. Tumor volumes were calculated using the elliptical formula: ½(length x width^2). Upon conclusion of the study, mice were euthanized following the Ethics Committee guidelines using isoflurane, and tumors were fixed (on 10% neutral-buffered formalin, then transferred into 70% ethanol) and processed for histological and sequencing analysis. We ensured that the tumors were collected on week 4 to prevent any animal fatalities resulting from severe tumor growth and declining health. The Department of Histology and Immunohistochemistry Laboratory performed hematoxylin and eosin (H&E) staining and provided the unstained slides.

Cell proliferation assay

Cell viability was performed using Cell Proliferation ELISA, BrdU (colorimetric) kit from Roche (Basel, Switzerland). Cells are cultured in the presence of the respective test substances in a 96-well plate at 37 °C for 24 hours. During this labeling period, the pyrimidine analog BrdU is incorporated in place of thymidine into the DNA of proliferating cells. Subsequently, BrdU is added to the cells, and the cells are incubated again for 24 hr. After removing the culture medium, the cells are fixed, and the DNA is denatured in one step by adding FixDenat (the denaturation of the DNA is necessary to improve the accessibility of the incorporated BrdU for detection by the antibody). The anti-BrdU-POD binds to the BrdU incorporated in newly synthesized cellular DNA. The subsequent substrate reaction detects the immune complexes. The reaction product is quantified by measuring the absorbance at the respective wavelength using a scanning multiwell spectrophotometer (ELISA reader). The developed color and absorbance directly correlate to the amount of DNA synthesis. BMDM cell proliferation after treatments with Mg^{2+} was assessed by measuring the serial halving of cell fluorescence intensity via flow cytometry. The CFDA-SE Cell Proliferation Assays (AlexaFluor488; Bio-Rad, USA) were used according to the manufacturer's protocol. After being placed in the appropriate conditions for cell proliferation, cells are harvested, sorted, and analyzed by LSRII (BD Pharmigen, San Jose, CA, USA).

Cell viability assay

Cell viability was measured using 3-[4,5-dimethylthiazol-2-yl]-2,5-diphenyl tetrazolium bromide (MTT) (Sigma-Aldrich, USA) according to the manufacturer's protocol. Cell viability was measured using the MTT method. Cells were seeded in 96-well plates at a density of 0.5×105 cells/well

and grown for 24 hours. 10 µL of MTT reagent (5 mg/ml MTT in PBS) was added to each well and incubated in a CO2 incubator for 4 hours. The resulting formazan dye was extracted with 100 µL of 0.01 N HCl in isopropanol, and within an hour, the absorbance was on an ELISA plate reader with a test wavelength of 570 nm and a reference wavelength of 630 nm. Cell viability was expressed as a percentage of the control culture.

Magnesium measurement and electrophysiology

For Imaging experiments, differentiated cells that were grown on glass bottom coverslips were incubated with 2 µM Mag-Fura 2-AM (Invitrogen) for the measurement of intracellular Mg^{2+} or with Fura-2 (Molecular Probes for 45 min) for the measurement of intracellular Ca^{2+}. After loading cells were washed twice with SES (Standard External Solution that includes: 10 mM HEPES, 120 mM NaCl, 5.4 mM KCl, 1 mM $MgCl_2$, 10 mM glucose, pH 7.4) buffer. For fluorescence measurements, the fluorescence intensity of Fura-2 or Mag-FURA-loaded cells was monitored with a CCD camera-based imaging system linked with an Olympus XL70 inverted fluorescence microscope. Fluorescence traces from individual cells imaged was obtained and the data shown represent $[Mg^{2+}]i$ values that are average from at least 30–40 cells. Also, the data presented are representative of at least 3–4 individual experiments performed in duplicate. Mg^{2+} or Ca^{2+} concentrations in individual cells were estimated by evaluating the 340/380 ratio as described before[57]. The patch pipette had resistances between 3-5 m after filling with the standard intracellular solution that contained the following (mM): cesium methane sulfonate, 145; NaCl, 8; $MgCl_2$, 10; HEPES, 10; EGTA, 10; pH 7.2 (CsOH). The maximum peak currents were calculated at a holding potential of -80 mV. The I/V curves were made using a ramp protocol where current density was evaluated at various membrane potentials and plotted. Blood was collected in heparin-containing collection tubes and separated into plasma by centrifugation at 3,000 *g* for 20 minutes at 4 °C. Mg^{2+} levels were determined with the QuantiChrom Magnesium Assay Kit (BioAssay System) by following the manufacturer's instructions. Briefly, plasma samples and dilutions of a standard Mg^{2+} solution (0, 0.2, 0.4, 0.6, 0.8, 1.0, and 1.2, 1.4, 1.6 and 2 mmol/l) were mixed with detecting reagents in microplates and incubated for 2 minutes at room temperature. The optical density (OD) was read at 500 nm. Then, EDTA solution was added, and the OD was read again at 500 nm to obtain background absorbance. Mg^{2+} concentration was calculated as $([OD_{sample} - OD_{blank}]/[OD_{Mg} - OD_{Mgblank}] \times 2$ [mg/dL]). OD_{sample} and OD_{blank} were sample absorbance values before and after the addition of EDTA. OD_{Mg} and $OD_{Mgblank}$ were OD values of the standard before and after the addition of EDTA.

Protein extractions and Western blotting

Whole-cell protein lysates were prepared in lysis buffer (10 mM Tris,140mMNaCl,1%NP-40, 0.5% SDS, and protease inhibitors, pH 8.0), protein concentrations were determined using the Bradford reagent (Bio-Rad Laboratories, USA), and 25–50 ug of protein were resolved on NuPAGE Novex 4–12% BisTris gels, transferred to PVDF membranes The membrane was blocked with skim milk in PBST solution and incubated with antibodies (Cell Signaling, MA, USA). After washing with PBST, secondary antibodies (Cell Signaling, MA, USA) were applied and detected by the Clarity Western ECL Substrate and Clarity Max Western ECL Substrate (Bio-Rad Laboratories, Hercules, CA, USA). Analysis and results were corrected for protein loading by normalization for β-actin expression. Densitometric analysis was performed using ImageJ analysis, and results were corrected for protein loading by normalization for β-actin (Cell Signaling, 4970S) as previously described[58]. Blot stripping was performed whenever necessary, using Restore PLUS Western Blot Stripping Buffer (Thermo Fisher, Waltham, MA, USA). The blots were washed with PBS Tween 20 (Sigma, USA), immersed in stripping buffer, and then incubated for 5-15 min at room temperature, then the stripping buffer was removed, and the blot was washed again and blocked for another 30 minutes before incubation with new antibody. The following primary antibodies (dilution accordingly by manufacturer's protocol) were used for western blot analysis: anti-NFκB p65 (p65) (Cell Signaling, 8242S), anti-pNFκB p65 (pp65) (Cell Signaling, 3033S), anti-STAT1 (Cell Signaling, 14994S), anti-pSTAT1 (Cell Signaling, 9167S), anti-STAT6 (Cell Signaling, 5397S), anti-p-STAT6 (Cell Signaling, 56554S), anti-iNOS (Cell Signaling, 13120S), anti-Arginase 1 (Cell Signaling, 93668S), anti-TRPM7 (Abcam, ab245408), anti-MAGT1 (Invitrogen, PAS-24978), anti-TRPM6 (Abcam, ab47017). Goat anti-rabbit IgG (Cell Signaling, 7074S), goat anti-mouse IgG (Cell Signaling, 7076S), and rabbit anti-Guinea IgG (H + L) were used as secondary antibodies. Appropriate antibody dilution was used according to the manufacturer's protocol.

Measurement of cytokines levels

IL-6, IL-1β, IFN-γ, IL-4, and IL-10 levels in the supernatant were measured using the Enzyme-Linked ImmunoSorbent Assay (ELISA) kit (Life Technologies, Carlsbad, CA, USA) following the manufacturer's instructions using standard diluent buffers designed for use with mouse serum. All samples were measured on a single 96-well plate for each cytokine, the cultured medium was centrifuged at 800x*g* for 5 min (4 °C), and the supernatant was used as the sample. Based on that criterion, all cytokine values for the bone marrow-derived macrophage serum samples examined were above the detection limit and within the reportable range of each assay.

Macrophage polarization and flow cytometer

On day 7, the formation of mature BMDM is evaluated using flow cytometry analysis and fluorophore-conjugated antibodies. Cells were resuspended with FACS buffer (PBS supplemented with 0.2% BSA), then blocked with Anti-Mouse CD16/CD32 Fc Blocker (BD Pharmigen, San Jose, CA, USA) for 15 minutes. After blocking, cells were tested for the expression of Anti-CD11b antibody [M1/70] (PE/Cy5®) (Abcam, Burlingame, CA, USA) and F4/80 Monoclonal Antibody (BM8), Pacific Blue (Thermo Fisher, Waltham, MA, USA) for macrophage line confirmation. For M1 macrophages, cells were stained with Anti-Mouse CD80 PE (eBioscience, San Diego, CA, USA); for M2 macrophage cells were stained with Anti-Mouse CD206 APC (eBioscience, San Diego, CA, USA). Cells were incubated for 30 min at 4 °C, then quantified on a BD LSR II (BD Pharmigen, San Jose, CA, USA). For polarization stimulation, BMDM was exposed to IFN-γ (20 ng/ml, Peprotech, Rocky Hill, NJ, USA) to generate the M1 phenotype and IL4 (20 ng/ml, Peprotech, Rocky Hill, NJ, USA) to generate the M2 phenotype. Stimulated cells were removed from wells and incubated in anti-mouse BD Fc Block CD16/CD32 (BD Biosciences, San Jose, CA) for 30 minutes on ice in FACS buffer (PBS with 3% FBS), then surface stained with antibodies for surface markers CD80 (Abcam, Cambridge, UK) and CD206 (Abcam, Cambridge, UK) for 15 min at 4 °C, following manufactory's protocol then analyzed by LSRII (BD Biosciences, San Jose, USA) and Cytek Autora (Cytek, California, USA) and FlowJo software version 9.0.

Measurement of mitochondrial oxygen consumption rate

Bone marrow-derived macrophages (BMDM) from WT mice (n = 3) were plated on 96-well Agilent Seahorse XF Cell culture microplates at a density of 4×10^5 cells per well. The macrophages were plated in their normal growth media overnight. The plated macrophage naive macrophages (M0) from WT were polarized to become pro-inflammatory macrophages (M1) and anti-inflammatory macrophages (M2) upon Interferon-γ (IFN-γ) or interleukin-4 (IL-4) stimulation for 24 hours. After polarization, the media was changed to Seahorse XF Cell Mito Stress Test Kit (Agilent) assay media supplemented with glucose, glutamine, and pyruvate concentrations equivalent to that of the growth media. Naïve Mφ, M1, and M2 macrophages were treated with no Mg^{2+} media and media containing 20 mM Mg^{2+} and with the SOCE channel inhibitor 2-ABP (10 µM) overnight, and oxygen consumption rate (OCR) was measured at 37 °C in an XF96 extracellular flux analyzer (Seahorse Bioscience, Agilent), which had been previously calibrated using Seahorse XF Calibrant solution (Seahorse Bioscience, Agilent) in a CO^2-free incubator overnight. Respiratory chain inhibitors were then loaded into the XF96 flux analyzer and added sequentially to cells at indicated time points. M0, M1, and M2 macrophages

received oligomycin (2 μM), FCCP (5 μM), and a mixture of antimycin A and rotenone (1 μM) sequentially[59]. Data were collected using Agilent Seahorse Wave 2.6.1 Desktop software and exported to GraphPad Prism version 8 for analysis.

Measurement of macrophage basal $_{m}Mg^{2+}$ in the permeabilized cell system

Naive primary macrophages derived from WT mice bone marrow were polarized to mature into M1 and M2 phenotypes using IFN-γ (20 ng/mL for 24 h) and IL4 (20 ng/mL for 24 h), respectively. After 24 h of polarization, the macrophages were washed in Ca^{2+} and Mg^{2+} free DPBS, pH 7.4. An equal number of cells (~ 3 x 10^6 cells) in the presence and absence of 20 mM Mg^{2+} for 1 h were resuspended and permeabilized with 40 μg/mL digitonin in 1.5 mL of intracellular medium (ICM) composed of 120 mM KCl, 1 mM KH_2PO4, 10 mM NaCl, 20 mM HEPES-Tris PH 7.2. The measurement of basal mMg^{2+} was performed by loading the permeabilized macrophages with Mag-Green (1 μM; Ex: 505 nm/Em: 535 and 595 nm)[59]. The spectrofluorimetric runs were performed at 37°C with constant stirring in the presence of 1.5 μM K^+-ATP and 5 mM succinate. A single bolus of the mitochondrial uncoupler, FCCP (10 μM), was added at the indicated time point. Fluorescence measurements were recorded in a multi-wavelength excitation dual-wavelength emission spectrofluorometer (Delta RAM, PTI, HORIBA). $_{m}[Mg^{2+}]_{out}$ is represented as f.a.u. of Mag-Green fluorescence (ex/em 505/595)[59].

Confocal microscopy

Laser confocal scanning microscopy (LASX Life Science microscope; Leica Microsystems) was used for single immunofluorescence staining to evaluate the expression of iNOS (Cell Signaling, iNOS (D6B6S) Rabbit mAb) and Arginase-1 (Cell Signaling, D4E3M, Rabbit mAb). Slides with fixed tumor cells were stained following manufacture protocol. Cells were blocked with horse serum (ThermoFisher, MA). The cells were counterstained with DAPI antifade mounting medium (2 mg/ml; ThermoFisher, MA) and observed with Laser confocal scanning microscopy. The immunofluorescence staining procedure was repeated three times.

RNA Sequencing and data analysis

Bone marrow derived macrophages (BMDM) were obtained from C57BL6/J wild-type (WT) 8-10-week-old male mice (The Jackson Laboratories, Bar Harbor, ME, USA). Naïve macrophages cells were treated with IFN-γ (20 ng/ml) and IL-4 (20 ng/ml) to activate macrophage polarization and change the naïve phenotype to M1 and M2 respectively. Cells were then treated with different concentrations of Mg^{2+}, then snap frozen in Trizol and sent for RNA sequencing to Novogene (Sacramento, CA, USA) for RNA extraction, and library preparation. The original image data file from high-throughput sequencing platforms (such as Illumina) is transformed to sequenced reads by CASAVA base recognition (Base Calling). FastQC v0.12.1 (https://www.bioinformatics.babraham.ac.uk/projects/fastqc/) tool has been used for the assessment of raw-read and then trimming of raw reads was performed using Trimmomatic version 0.36 with parameters such as "LEADING:3 TRAILING:3 HEADCROP:15 MINLEN:30"[60]. Cleaned and good quality reads were mapped onto mm10 reference genome using HISAT2 tool with parameters "--rna-strandness RF"[61]. Aligned results were further used for reading count assessment using FeatureCounts[62]. Finally, the edgeR tool was used for the identification of differential expressed genes using p-value cutoff 0.05 for significant genes[63]. WebGestalt (WEB-based Gene SeT AnaLysis Toolkit), an online server has been used for pathways as well as gene ontology analysis of differential expressed genes[62].

Statistical analysis

Data analysis was performed using a one-way ANOVA or Student *t*-test on GraphPad prism 8.0. Calcium measurement and electrophysiology were analyzed using Origin 9.0. Experimental values are expressed as means ± SD. * indicates significance of $P < 0.05$, ** of $P < 0.01$ and *** of $P < 0.001$, respectively.

Data availability

The data supporting the findings of this study have been made available within the paper and its supplementary materials.

Received: 10 April 2024; Accepted: 19 January 2025;
Published online: 28 January 2025

References

1. Murray, P. J. et al. Macrophage activation and polarization: nomenclature and experimental guidelines. *Immunity* **41**, 14–20 (2014).
2. Wynn, T. A., Chawla, A. & Pollard, J. W. Macrophage biology in development, homeostasis and disease. *Nature* **496**, 445–455 (2013).
3. Kigerl, K. A. et al. Identification of two distinct macrophage subsets with divergent effects causing either neurotoxicity or regeneration in the injured mouse spinal cord. *J. Neurosci.* **29**, 13435–13444 (2009).
4. Castro-Dopico, T. et al. GM-CSF calibrates macrophage defense and wound healing programs during intestinal infection and inflammation. *Cell Rep.* **32**, 107857 (2020).
5. Lackey, D. E. & Olefsky, J. M. Regulation of metabolism by the innate immune system. *Nat. Rev. Endocrinol.* **12**, 15–28 (2016).
6. Werz, O. et al. Human macrophages differentially produce specific resolvin or leukotriene signals that depend on bacterial pathogenicity. *Nat. Commun.* **9**, 59 (2018).
7. Kubala, M. H. et al. Plasminogen activator inhibitor-1 promotes the recruitment and polarization of macrophages in cancer. *Cell Rep.* **25**, 2177–2191.e2177 (2018).
8. Van den Bossche, J., O'Neill, L. A. & Menon, D. Macrophage Immunometabolism: Where Are We (Going)? *Trends Immunol.* **38**, 395–406 (2017).
9. Tur, J., Vico, T., Lloberas, J., Zorzano, A. & Celada, A. Macrophages and mitochondria: a critical interplay between metabolism, signaling, and the functional activity. *Adv. Immunol.* **133**, 1–36 (2017).
10. Weinberg, S. E., Sena, L. A. & Chandel, N. S. Mitochondria in the regulation of innate and adaptive immunity. *Immunity* **42**, 406–417 (2015).
11. Hamers, A. A. J. & Pillai, A. B. A sweet alternative: maintaining M2 macrophage polarization. *Sci. Immunol.* https://doi.org/10.1126/sciimmunol.aav7759 (2018).
12. Dowling, J. K. et al. Mitochondrial arginase-2 is essential for IL-10 metabolic reprogramming of inflammatory macrophages. *Nat. Commun.* **12**, 1460 (2021).
13. Mosser, D. M. & Edwards, J. P. Exploring the full spectrum of macrophage activation. *Nat. Rev. Immunol.* **8**, 958–969 (2008).
14. Lotscher, J. et al. Magnesium sensing via LFA-1 regulates CD8(+) T cell effector function. *Cell* **185**, 585–602.e529 (2022).
15. Daw, C. C. et al. Lactate Elicits ER-Mitochondrial Mg(2+) dynamics to integrate cellular metabolism. *Cell* **183**, 474–489.e417 (2020).
16. Li, F. Y. et al. Second messenger role for Mg2+ revealed by human T-cell immunodeficiency. *Nature* **475**, 471–476 (2011).
17. Romani, A. M. Magnesium homeostasis in mammalian cells. *Front Biosci.* **12**, 308–331 (2007).
18. Kanellopoulou, C. et al. Mg(2+) regulation of kinase signaling and immune function. *J. Exp. Med.* **216**, 1828–1842 (2019).
19. Yamanaka, R. et al. Mitochondrial Mg(2+) homeostasis decides cellular energy metabolism and vulnerability to stress. *Sci. Rep.* **6**, 30027 (2016).
20. Feske, S., Wulff, H. & Skolnik, E. Y. Ion channels in innate and adaptive immunity. *Annu. Rev. Immunol.* **33**, 291–353 (2015).
21. Feske, S., Skolnik, E. Y. & Prakriya, M. Ion channels and transporters in lymphocyte function and immunity. *Nat. Rev. Immunol.* **12**, 532–547 (2012).
22. Deason-Towne, F., Perraud, A. L. & Schmitz, C. The Mg2+ transporter MagT1 partially rescues cell growth and Mg2+ uptake in cells lacking the channel-kinase TRPM7. *FEBS Lett.* **585**, 2275–2278 (2011).
23. Ryazanova, L. V. et al. TRPM7 is essential for Mg(2+) homeostasis in mammals. *Nat. Commun.* **1**, 109 (2010).

24. Ryazanova, L. V. et al. Elucidating the role of the TRPM7 alpha-kinase: TRPM7 kinase inactivation leads to magnesium deprivation resistance phenotype in mice. *Sci. Rep.* **4**, 7599 (2014).
25. Li, F. Y., Lenardo, M. J. & Chaigne-Delalande, B. Loss of MAGT1 abrogates the Mg2+ flux required for T cell signaling and leads to a novel human primary immunodeficiency. *Magnes. Res.* **24**, S109–S114 (2011).
26. Mastrototaro, L., Smorodchenko, A., Aschenbach, J. R., Kolisek, M. & Sponder, G. Solute carrier 41A3 encodes for a mitochondrial Mg(2+) efflux system. *Sci. Rep.* **6**, 27999 (2016).
27. Yi, L. et al. Macrophage colony-stimulating factor and its role in the tumor microenvironment: novel therapeutic avenues and mechanistic insights. *Front Oncol.* **14**, 1358750 (2024).
28. Nadler, M. J. et al. LTRPC7 is a Mg.ATP-regulated divalent cation channel required for cell viability. *Nature* **411**, 590–595 (2001).
29. Runnels, L. W., Yue, L. & Clapham, D. E. The TRPM7 channel is inactivated by PIP(2) hydrolysis. *Nat. Cell Biol.* **4**, 329–336 (2002).
30. Sun, Y. et al. Increase in serum Ca2+/Mg2+ ratio promotes proliferation of prostate cancer cells by activating TRPM7 channels. *J. Biol. Chem.* **288**, 255–263 (2013).
31. Gotru, S. K. et al. Cutting edge: imbalanced cation homeostasis in MAGT1-deficient B cells dysregulates B cell development and signaling in mice. *J. Immunol.* **200**, 2529–2534 (2018).
32. Li, M. et al. Molecular determinants of Mg2+ and Ca2+ permeability and pH sensitivity in TRPM6 and TRPM7. *J. Biol. Chem.* **282**, 25817–25830 (2007).
33. Jin, J. et al. Deletion of Trpm7 disrupts embryonic development and thymopoiesis without altering Mg2+ homeostasis. *Science* **322**, 756–760 (2008).
34. Zhang, Y. H. & Hancox, J. C. Gadolinium inhibits Na(+)-Ca(2+) exchanger current in guinea-pig isolated ventricular myocytes. *Br. J. Pharm.* **130**, 485–488 (2000).
35. Guinamard, R., Simard, C. & Del Negro, C. Flufenamic acid as an ion channel modulator. *Pharm. Ther.* **138**, 272–284 (2013).
36. Qiao, W. et al. TRPM7 kinase-mediated immunomodulation in macrophage plays a central role in magnesium ion-induced bone regeneration. *Nat. Commun.* **12**, 2885 (2021).
37. Martinez, F. O., Sica, A., Mantovani, A. & Locati, M. Macrophage activation and polarization. *Front Biosci.* **13**, 453–461 (2008).
38. Martinez, F. O. & Gordon, S. The M1 and M2 paradigm of macrophage activation: time for reassessment. *F1000Prime Rep.* **6**, 13 (2014).
39. Kimura, T. et al. Polarization of M2 macrophages requires Lamtor1 that integrates cytokine and amino-acid signals. *Nat. Commun.* **7**, 13130 (2016).
40. Orecchioni, M., Ghosheh, Y., Pramod, A. B. & Ley, K. Macrophage polarization: different gene signatures in M1(LPS+) vs. classically and M2(LPS-) vs. alternatively activated macrophages. *Front Immunol.* **10**, 1084 (2019).
41. Bosco, M. C. Macrophage polarization: Reaching across the aisle? *J. Allergy Clin. Immunol.* **143**, 1348–1350 (2019).
42. Corliss, B. A., Azimi, M. S., Munson, J. M., Peirce, S. M. & Murfee, W. L. Macrophages: an inflammatory link between angiogenesis and lymphangiogenesis. *Microcirculation* **23**, 95–121 (2016).
43. Diez-Tercero, L., Delgado, L. M., Bosch-Rue, E. & Perez, R. A. Evaluation of the immunomodulatory effects of cobalt, copper and magnesium ions in a pro inflammatory environment. *Sci. Rep.* **11**, 11707 (2021).
44. Mills, E. L. et al. Succinate dehydrogenase supports metabolic repurposing of mitochondria to drive inflammatory macrophages. *Cell* **167**, 457–470.e413 (2016).
45. Wang, F. et al. Glycolytic stimulation is not a requirement for M2 macrophage differentiation. *Cell Metab.* **28**, 463–475.e464 (2018).
46. Starostina, I. et al. Distinct calcium regulation of TRPM7 mechanosensitive channels at plasma membrane microdomains visualized by FRET-based single cell imaging. *Sci. Rep.* **11**, 17893 (2021).
47. Roy, S. et al. Redefining the transcriptional regulatory dynamics of classically and alternatively activated macrophages by deepCAGE transcriptomics. *Nucleic Acids Res.* **43**, 6969–6982 (2015).
48. Mircetic, R. N., Dodig, S., Raos, M., Petres, B. & Cepelak, I. Magnesium concentration in plasma, leukocytes and urine of children with intermittent asthma. *Clin. Chim. Acta* **312**, 197–203 (2001).
49. Ferioli, S. et al. TRPM6 and TRPM7 differentially contribute to the relief of heteromeric TRPM6/7 channels from inhibition by cytosolic Mg(2+) and Mg.ATP. *Sci. Rep.* **7**, 8806 (2017).
50. Krapivinsky, G., Krapivinsky, L., Manasian, Y. & Clapham, D. E. The TRPM7 chanzyme is cleaved to release a chromatin-modifying kinase. *Cell* **157**, 1061–1072 (2014).
51. Nadolni, W. & Zierler, S. The channel-kinase TRPM7 as novel regulator of immune system homeostasis. *Cells* https://doi.org/10.3390/cells7080109 (2018).
52. Pilchova, I., Klacanova, K., Tatarkova, Z., Kaplan, P. & Racay, P. The involvement of Mg(2+) in regulation of cellular and mitochondrial functions. *Oxid. Med. Cell Longev.* **2017**, 6797460 (2017).
53. Weischenfeldt, J. & Porse, B. Bone Marrow-Derived Macrophages (BMM): Isolation and Applications. *CSH Protoc* **2008**, pdb prot5080. https://doi.org/10.1101/pdb.prot5080 (2008).
54. Trouplin, V. et al. Bone marrow-derived macrophage production. *J Vis Exp*, e50966 (2013).
55. Gonzales, C. B. et al. Vanilloids induce oral cancer apoptosis independent of TRPV1. *Oral. Oncol.* **50**, 437–447 (2014).
56. De La Chapa, J. J. et al. The novel capsazepine analog, CIDD-99, significantly inhibits oral squamous cell carcinoma in vivo through a TRPV1-independent induction of ER stress, mitochondrial dysfunction, and apoptosis. *J. Oral. Pathol. Med.* **48**, 389–399 (2019).
57. Sun, Y., Kamat, A. & Singh, B. B. Isoproterenol-dependent activation of TRPM7 protects against neurotoxin-induced loss of neuroblastoma cells. *Front Physiol.* **11**, 305 (2020).
58. Singh, B. B. et al. VAMP2-dependent exocytosis regulates plasma membrane insertion of TRPC3 channels and contributes to agonist-stimulated Ca2+ influx. *Mol. Cell* **15**, 635–646 (2004).
59. Madaris, T. R. et al. Limiting Mrs2-dependent mitochondrial Mg2+ uptake induces metabolic programming in prolonged dietary stress. *Cell Rep*. https://doi.org/10.1016/j.celrep.2023.112155 (2023).
60. Bolger, A. M., Lohse, M. & Usadel, B. Trimmomatic: a flexible trimmer for Illumina sequence data. *Bioinformatics* **30**, 2114–2120 (2014).
61. Kim, D., Paggi, J. M., Park, C., Bennett, C. & Salzberg, S. L. Graph-based genome alignment and genotyping with HISAT2 and HISAT-genotype. *Nat. Biotechnol.* **37**, 907–915 (2019).
62. Liao, Y., Smyth, G. K. & Shi, W. featureCounts: an efficient general purpose program for assigning sequence reads to genomic features. *Bioinformatics* **30**, 923–930 (2014).
63. Robinson, M. D., McCarthy, D. J. & Smyth, G. K. edgeR: a Bioconductor package for differential expression analysis of digital gene expression data. *Bioinformatics* **26**, 139–140 (2010).

Acknowledgements

This work was funded by grant support from the National Institutes of Health (R01DE017102; R01DE022765) awarded to B.B.S and (R01GM109882, R01DK135179, and R01HL142673) awarded to M.M. T.R.M. is supported by the NIH (R01GM109882-S1 and T32 AG 021890).The funders had no further role in the study design, data analysis, and/or interpretation of the data. Flow Cytometry Facility is supported by UTHSCSA, NIH-NCI P30 CA054174-20, and UL1 TR001120. We also thank Dr. Cara Gonzales (Department of Comprehensive Dentistry- UTHSCSA) for providing the female athymic nude mice for the tumor model.

Author contributions

Conceptualization, methodology, and analysis, V.C., T.R.M., B.B.M. M.M and B.B.S., Investigation, V. C., Y.S., V. D., R., J., X., C., K.R., M.V., J.D., L.C., Writing–Review and Editing, V.C., T.R.M., B.B.S. M.M.

Competing interests
The authors declare no competing interests.

Additional information
Supplementary information The online version contains supplementary material available at https://doi.org/10.1038/s41698-025-00815-x.

Correspondence and requests for materials should be addressed to Muniswamy Madesh or Brij B. Singh.